2023

The Wound Healing and Antibacterial Properties of Mesenchymal Stromal Cell Extracellular Matrix Nanoparticles

Emily N. Wandling
Virginia Commonwealth University

The Wound Healing and Antibacterial Properties of Mesenchymal Stromal Cell Extracellular Matrix Nanoparticles

A thesis submitted in partial fulfillment of the requirements of the degree of Master of Science in Biomedical Engineering at Virginia Commonwealth University.

By Emily N. Wandling

B.S. Biochemistry and Molecular Biology, Sweet Briar College, 2020

Director: Rebecca L. Heise, Ph.D.,

Associate Professor, Department of Biomedical Engineering

Virginia Commonwealth University

Richmond, Virginia

May 2023

Table of Contents

Abstract

Treatments for acute respiratory distress syndrome (ARDS) are still unavailable and the prevalence of the disease has only increased due to the Covid-19 pandemic. Mechanical ventilation regiments are still utilized to support declining lung function, but they also contribute to lung damage and increase the risk of bacterial infection. The anti-inflammatory and pro-regenerative abilities of mesenchymal stromal cells (MSCs) have shown to be a promising therapy for ARDS. We propose to utilize the regenerative effects of MSC secretome and the extracellular matrix (ECM) into a nanoparticle. Our mouse MSC (MMSC) ECM nanoparticles were characterized using size, zeta-potential, and mass spectrometry to evaluate their potential wound healing and antimicrobial abilities. The nanoparticles had an average size of 273.4 nm (±25.6) while possessing a negative zeta-potential, allowing them to surpass defenses and reach the distal regions of the lung. It was found that the MMSC ECM nanoparticles were biocompatible with MLE-12 and MMSCs, accelerate the wound closure of human lung fibroblasts, while inhibiting the growth of *Pseudomonas aeruginosa,* a common lung pathogen. Our MMSC ECM nanoparticles display characteristics of healing injured lungs while preventing bacterial infection that can increase recovery time.

Acknowledgments

I would first like to thank my family for encouraging and supporting me while completing this project. Next, I would like to thank my mentor Dr. Heise. I am so grateful for your amazing advice, encouragement, and support during this project and in the future. I would like to give a big thank you to Keera Rhoads, for assisting me with running experiments during this project. Thank you to the other students in the Heise Lab, for your advice and help with experiments.

For assistance conducting experiments for this project, we appreciate the Da Rocha Lab at Virginia Commonwealth University for their help obtaining the size and zeta-potential of our MMSC ECM Nanoparticles. A big thank you to Dr. Dennis Ohman for letting us use your lab space and help conducting bacterial assays. We also acknowledge the Biomolecular Analysis Facility at the University of Virginia for their acquisition of the mass spectrometry data.

I would also like to thank the Graduate Program at Virginia Commonwealth University, for awarding me the Graduate School Fellowship Scholarship, which helped support my degree. Finally, thank you to my committee members for their advice and guidance about this project.

List of Abbreviations and Symbols

ACE-2	Angiotensin-converting enzyme 2
ALI	Acute Lung Injury
AMPs	Antimicrobial Peptides
ARDS	Acute Respiratory Distress Syndrome
CARDS	COVID-10 associated Acute Respiratory Distress Syndrome
COVID-19	Coronavirus SARS-CoV2
dECM	Decellularized Extracellular Matrix
DMEM	Dulbecco's Modified Eagle Medium
DNA	Deoxyribonucleic Acid
ECM	Extracellular Matrix
GAGs	Glycosaminoglycans
HBSS	Hank's Balanced Salt Solution
IL-1	Interleukin-1
IL-1β	Interleukin-1 beta
IL-6	Interleukin 6
IL-10	Interleukin 10
KGF	keratinocyte growth factor
LB broth	Luria-Bertani Broth
MLE-12	Mouse Lung Epithelial
MSCs	Mesenchymal Stromal Cells
MMSCs	Mouse Mesenchymal Stromal Cells
PBS	Phosphate-buffered saline
PL	Pig Lung

SEM	Scanning Electron Microscopy
TGF-β	Transforming growth factor beta
TNF-α	Tumor Necrosis Factor-alpha
VAP	Ventilator-associated pneumonia

List of Figures

List of Tables

Introduction

1. Lung Disease

1.1 Acute Respiratory Distress Syndrome

Acute lung injury (ALI) and the more severe acute respiratory distress syndrome (ARDS) remain life-threatening conditions to patients worldwide. ARDS is categorized into three stages: exudative, proliferative, and fibrotic depending on disease progression (1). ARDS is characterized by an influx of inflammatory cells as a response to an injured lung. The inflammatory response leads to progressive alveolar damage and increased fluid, protein, neutrophil, and blood cell permeability in the lung epithelium (2). Over time, the damage causes necrosis of lung epithelial cells, resulting in gaps in the epithelial barrier which lowers the efficiency of gas exchange (3). The progressive injury of the lung due to the inflammatory response leads to pulmonary edema, hypoxemia, and pulmonary fibrosis, which can ultimately culminate to respiratory failure (4).

ARDS is most prevalent in patients that are critically ill with comorbidities, including sepsis and pneumonia. Development of ARDS may also occur through inhalation of toxins, such as chlorine and phosgene gasses, due to trauma to the head, chest, or brain (2). Disease progression of ARDS can begin up to seven days after the etiological incident. There are approximately three million patients with ARDS every year. Out of these cases, 10% consist of patients in the intensive care unit (5). The mortality rate of ARDS continues to remain high at 43% (6).

Currently, there are not any pharmacological treatments to cure ARDS (7). Treatments and care regiments are used to mitigate symptoms such as mechanical ventilation, which is used to supply oxygen to the patient's airspaces, anti-inflammatory medications, antibiotics to treat infection, diuretics to remove excess fluid from the lungs, and sedative medications to relieve

pain from shortness of breath (8). Approximately 24% of ARDS patients receive mechanical ventilation treatment, which can contribute to an already inflammatory lung environment (9). Mechanical ventilation may also induce ventilator-associated pneumonia (VAP) from inhalation of a microbial pathogen on a contaminated ventilator unit (10).

1.2 Pathophysiology of Acute Respiratory Distress Syndrome

1.2.1 Exudative Phase

The exudative phase of ARDS begins with the activation of alveolar macrophages due to the inciting lung injury or infectious agent. An inflammatory response stimulated by the release of pro-inflammatory cytokines, including IL-1β, TNF-α, IL-6, and IL-8, are upregulated by the macrophages to recruit neutrophils to the site of the injury (11,12). Other inflammatory bioactive molecules, such as reactive oxygen species, phospholipids, and proteases, are attracted to the injury site to perpetuate the inflammatory response (11).

Infiltration of neutrophils results in damage to the vascular endothelial and alveolar epithelial barriers. Damage to the endothelial barrier may also occur through activation by the pro-inflammatory cytokines released by macrophages. Activated endothelial cells can cause neutrophil-platelet aggregates to deposit on the endothelial cell layer (2). All of these factors cause an increase in the permeability of the endothelial vasculature and allow easier entry of inflammatory cells and cytokines into the alveolar epithelial space. This results in the necrosis of type I alveolar epithelial cells, which compose of the surface for gas exchange and type II alveolar epithelial cells, which are responsible for the production of surfactant and healing of the epithelial barrier after injury (13). Surfactant is a phospholipid protein complex that promotes compliance of the lung tissue, allowing for easier inflation and oxygen uptake. Surfactant is also a defense against bacterial and viral infections (14). As the pro-inflammatory response continues

to circulate, alveolar cell necrosis produces gaps in the epithelial barrier, contributing to the increased vascular permeability. Inflammatory edema fluid, containing immune cells and inflammatory cytokines, begins to easily flow into the alveolar space (12). The end result of this phase is pulmonary edema, reduction of surfactant production, and deposition of cell debris forming a hyaline membrane over the alveolar epithelium, which decreases lung compliance and inhibits gas exchange (3,15).

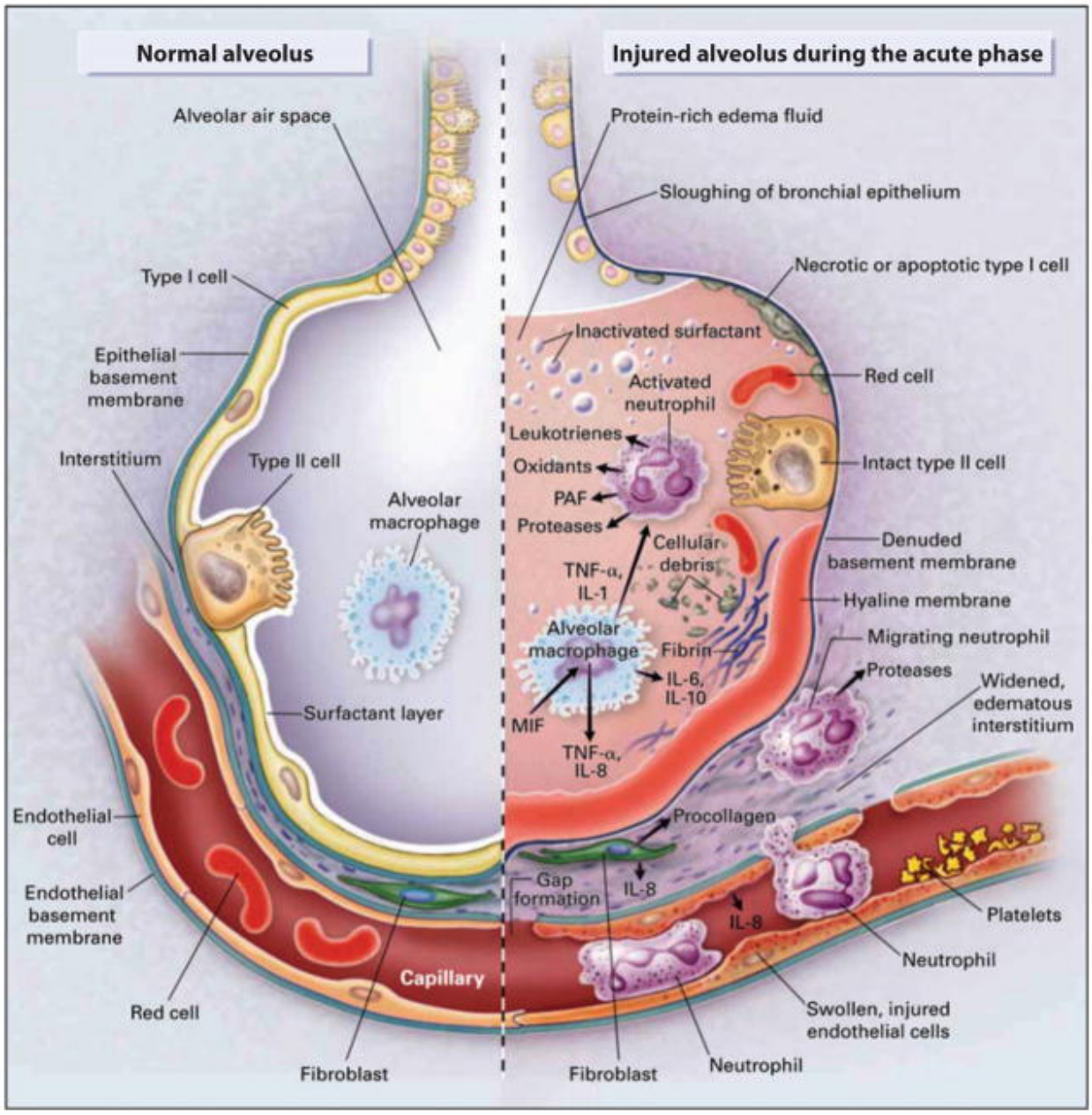

Figure 1. The normal and the injured alveolus during the acute phase of ARDS (17).

1.2.2 Proliferative Phase

The proliferative phase of ARDS begins approximately two to three weeks after the inciting injury which stimulated the exudative phase. This phase initiates the process of lung repair by suppressing pro-inflammatory cytokine production (3). Macrophages are responsible for removing damaged host cells and debris from the alveolar space, releasing anti-inflammatory factors IL-10 and TGF-β (16). Fluid is removed from the alveolar space as alveolar ion channels and aquaporins are expressed and activated (3). The immune response shifts to a healing phase by removing neutrophils and recruitment of fibroblasts that deposit collagen and repair the extracellular matrix (17). In an attempt to recover the structure of the lung, new alveolar epithelium is grown from type II alveolar epithelium differentiating into the type I alveolar epithelium that comprises the layer for gas exchange (12). In some patients, the resolution of ARDS occurs once pulmonary edema and acute inflammation are terminated (17).

However, a prolonged immune response during the proliferative phase may cause further trouble for a patient with severe ARDS, marked as an excessive proliferation of fibroblasts to the alveolar space. This may lead to pulmonary fibrosis, the remodeling of the lung architecture with stiff and scarred fibrotic lung tissue (16).

1.2.3 Fibrotic Phase

Pulmonary fibrosis, also called the fibrotic phase, is considered to be the final pathological stage of ARDS. Pulmonary fibrosis is characterized by abnormal repair of lung tissue, resulting in scarred, thickened lung tissue, and contorted alveolar space (18). The final phase increases the risk of mortality, as fibrosis is the cause of respiratory death for 40% of patients (19). Patients are often ventilator dependent, as the thickened lung tissue and irregularly shaped alveolar spaces decrease lung compliance and cause hypoxemia (20). An overabundance of fibroblasts during the proliferative phase contributes to the development of fibrotic tissue (21).

The overproduction of ECM components collagen, fibronectin, growth factors, and glycoproteins, and remodeling of the lung architecture develop into fibrotic lung tissue (22). The proinflammatory cytokines, including TNF-α and IL-1β, recruited at the beginning of lung injury tend to be present during the fibrotic stage of ARDS. If uncleared by the macrophages in the proliferation phase, the persistence of these cytokines in the injured lung may be the cause of fibrosis, as TNF-α and IL-1β are chemotactic for lung fibroblasts and stimulate cellular collagen synthesis (19).

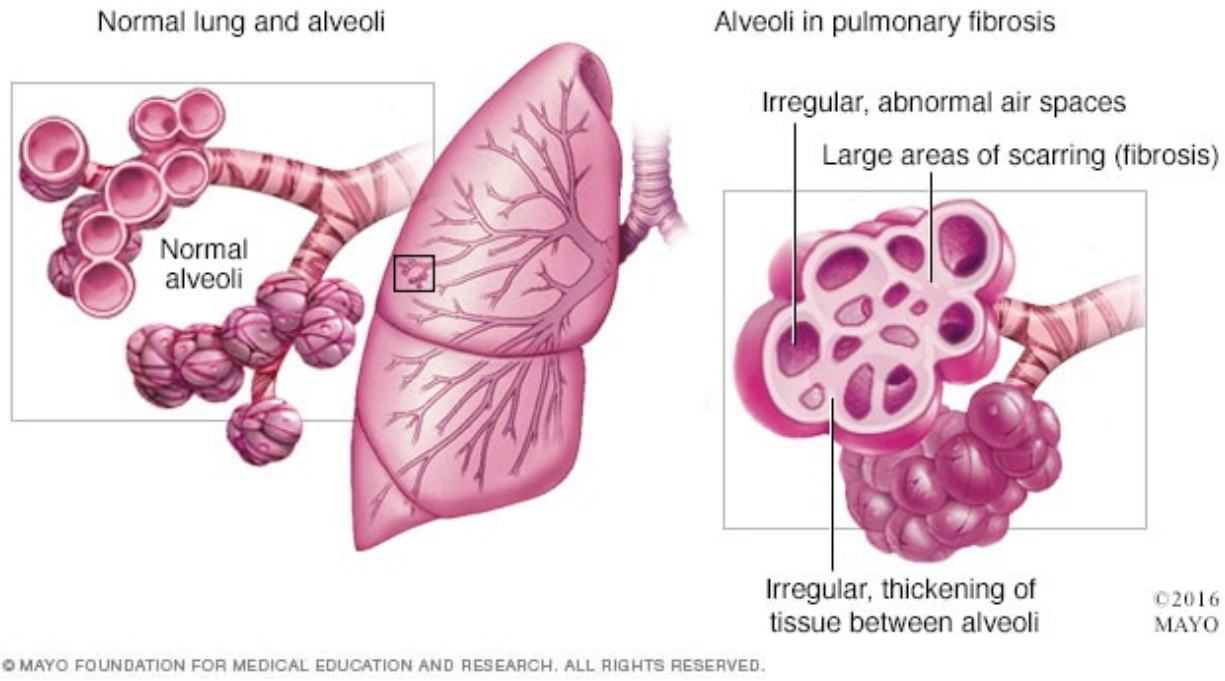

Figure 2. Alveolar Structure in Healthy Lung vs Pulmonary Fibrosis Lung (23).

1.3 Acute Respiratory Distress Syndrome and SARS-CoV-2

The frequency of ARDS in critically ill patients has only continued to increase due to the Coronavirus, SARS-CoV-2, pandemic that began in 2019. Infection with the Coronavirus (COVID-19) begins with damage to the respiratory endothelial layer (24). It is proposed that SARS-CoV-2 binds to the ACE-2 receptor on alveolar type II cells. As the virus continues to

replicate and infiltrate the alveolar type II cells, it causes the inhibition of surfactant production leading to tissue inflammation, alveolar cell necrosis, and hypoxemia (24). This leads to an increase in pro-inflammatory response causing diffuse alveolar damage and increased interstitial edema that is characteristic of the progression to developing ARDS (25).

About 33% of hospitalized patients with COVID-19 develop ARDS, denoted as COVID-19-associated ARDS (CARDS) (25). Of those hospitalized patients, 75% of intensive-care patients that have severe COVID-19 symptoms develop ARDS (26). The majority cause of mortality from COVID-19 was cited to be acute respiratory failure caused by ARDS. Similarly, to ARDS, the treatment of CARDS consists of using mechanical ventilation to support lung function, although ventilation regiments may be modified due to the high lung compliance of patients with CARDS compared to classic ARDS (27).

1.4 Mechanical Ventilation and Ventilator-induced Lung Injury

As mentioned previously, the standard treatment for patients with ARDS effected by declining lung function is mechanical ventilation. However, ventilation can also contribute to the damage and inflammatory environment in the injured lung from the excessive mechanical force the ventilator exerts (28). Ventilator-induced lung injury is the condition used to describe the inflammation and destruction of lung tissue during mechanical ventilation (29). The elevated pressure from ventilation can lead to volutrauma, excessive inflation of the lung, and barotrauma, leakage of air in the lungs, causing alveolar distention and breakage in the alveolar wall respectively (30). Alveolar damage is furthered from atelectrauma, the repetitive opening of the alveoli during ventilation. Biotrauma describes the stimulation of inflammatory molecules in response to the induced volutrauma (31). High-pressure volume ventilation strategies are known

to produce a shear force that is capable of removing cells at the epithelial and endothelial membrane, furthering vascular permeability and infiltration of inflammatory cells. To decrease lung injury during mechanical ventilation, lung protective strategies, such as lowering the driving pressure of the ventilator, have shown to reduce ventilator-induced damage to the lungs, but there is still a need to decrease the duration of ventilation (28)

1.5 Ventilator-Associated Pneumonia

Another risk associated with mechanical ventilation is the development of VAP (32). VAP can occur beginning 48-72 hours into ventilation therapy and manifests as fever, respiratory distress, and the presence of white blood cells in the tracheal aspirate (33). VAP is one of the most frequently acquired infections in the ICU, as 27% of patients in critical care are affected by VAP and 86% of pneumonia cases developed in the hospital are due to mechanical ventilation (10). Between 20% and 40% of patients with ARDS will experience complications with VAP. VAP increases the length of care in the ICU from 4 days up to 13 days and increases the risk of mortality for a patient with ARDS reportedly up by 13% (10, 35). Typically, the pathogen that causes VAP is bacterial, as viral and fungal VAP diagnoses are rare (36).

The acquisition of VAP is believed to be caused by the infiltration of bacteria into the upper airway, leading to bacterial colonization in the trachea. Bacterial pathogens can enter the airways through contamination of equipment or aspiration of bacterial secretions into the ventilation equipment (36). The usage of an endotracheal tube increases the risk of colony formation, as the bacteria can lodge within the tube during treatment (35). The colonizing bacteria are not cleared from the lungs as the patient's innate and adaptive immune system is already occupied with inflammation from ARDS (37). Additionally, the immune defense of the

alveoli is weakened by mechanical defenses inflicted by intubation. Mucus secretion and ciliary motion are inhibited by ventilation, preventing clearance of bacterial infection, and allowing for colonization and the formation of a biofilm. Preoccupation and impairment of the immune defenses eventually escalate, and the initial bacterial infection develops into pneumonia (33).

The most common pathogens of VAP include gram-negative *Pseudomonas aeruginosa*, *Klebsiella pneumoniae*, *Enterobacter cloacae,* and *Acinetobacter baumannii*, making up approximately 50% of all VAP diagnoses. *Staphylococcus aureus* was mentioned as a frequent gram-positive pathogen that caused a VAP infection (38). VAP may be caused by one bacterial pathogen or considered polymicrobial infection if caused by two or more bacteria (39). Currently, the most utilized method for treating VAP is antibiotic therapy. It is critical that the initial antimicrobial therapy be effective against the pathogen, or else ventilation time may be extended, or the infection may become drug-resistant (40). Unfortunately, due to the frequent use of antibiotics to treat infection, there has been a rapid increase in the development of bacterial strains that can resist antibiotic treatment (41).

1.5.1 Antibiotic Resistance

Due to the increased use of antibiotics in medical care, there has been a case of resistance for almost every antibiotic that has been used as a treatment. Along with the overuse of antibiotics, the utilization of antibiotics in agriculture and the lack of development in new antibiotics have contributed to the rise of bacteria resistance to antibiotics (42). Additionally, exposure to antibiotics increases the risk that the patient will obtain a multi-drug resistant infection rate (37). Acquiring an infection with an antibiotic-resistant bacterium is known to increase the mortality rate, intensive care treatment, and healthcare costs for the patient (43). Antimicrobial resistance has reportedly risen during the COVID-19 pandemic for *P. aeruginosa*,

S. aureus, and *K. pneumoniae*, common pathogens involved with VAP (38). The opportunistic pathogen, *P. aeruginosa*, is a pathogen of concern in regard to antibiotic resistance. Due to its large genome, high adaptability, and biofilm formation, *P. aeruginosa* is able to effectively resist antibiotic treatments (44). Out of the VAP diagnosis from COVID-19, nearly 66.67% of infections were caused by multi-drug resistant pathogens (45). This alarming increase in antibiotic-resistant bacteria strains proves there is an urgent need to develop novel therapies to prevent lung infection and damage.

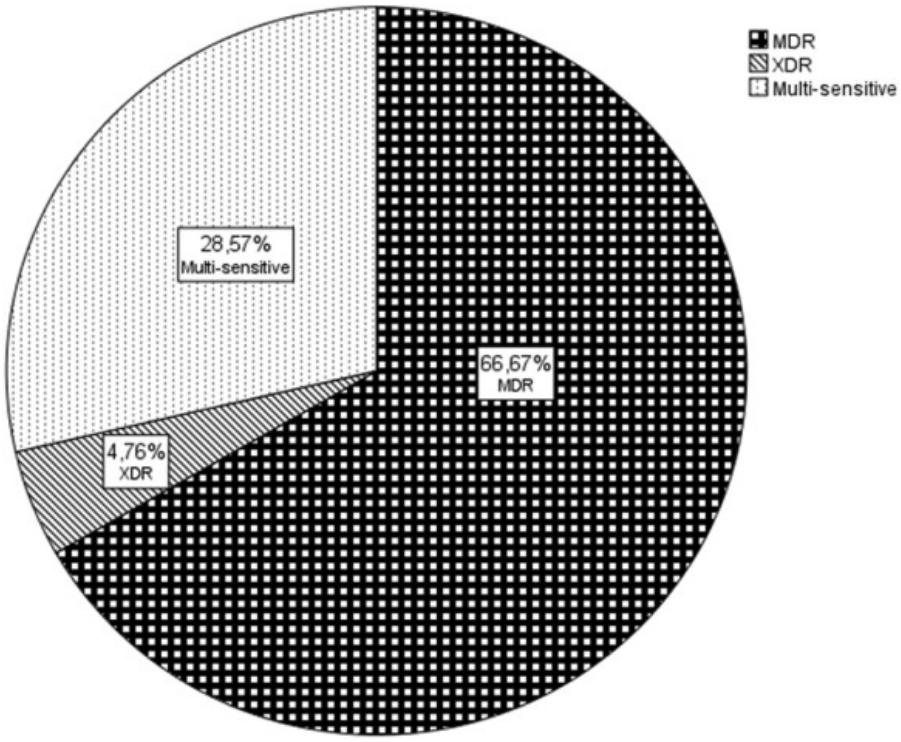

Figure 3. Cases of Bacterial Resistance in VAP; MDR: multidrug-resistant; XDR: extreme-drug resistant (45).

2. Treatments for Lung Disease

2.1 Aerosol Treatment Delivery to Lung Injury and Bacterial Infection

The most common method of delivering treatments to the lungs is through the use of aerosolized particles administered by inhalation. Inhalation of the treatment is a non-invasive procedure that allows delivery of the treatment to the alveoli, allowing for the drugs to be absorbed by the blood through diffusion. The dose of drug delivery can also be controlled using the method of inhalation, through immediate-release or controlled-release of the drug system. Before accessing the target lung epithelium, the drugs must avoid biological barriers used to clear foreign pathogens from the environment (46). Under inflammatory conditions induced by ARDS and bacterial infection, these defenses will be exacerbated.

The mucociliary barrier consists of cilia on the surface of airway epithelial cells and a layer of mucous composed of mucopolysaccharides. Inhaled particulates are captured in the mucous layer and expelled through the respiratory tract. Another barrier is a pulmonary surfactant, a lipoprotein complex of phospholipids and surfactant protein secreted by alveolar type II cells that particles can deposit in. Pulmonary macrophages can recognize the foreign inhaled treatment, inducing phagocytosis and an inflammatory response to the drug. During bacterial infection, a biofilm layer may be produced by the colony to serve as a barrier against inhaled treatments (47).

Inhaled nanoparticle medicines have been explored for treating chronic and acute lung diseases. Nanoparticles with a size lower than 5 μm have been shown to encourage deposition of treatment in the lungs and improve solubility. Nanosized delivery systems that contain bioactive molecules have displayed uniform distribution in the lung as well as producing a minimal immune response. Nanoparticle delivery systems composed of liposomes and dendrimers have already shown promise in treating ARDS (48). With the correct size, charge, and bioactive

components, a nanoparticle can be developed as an inhaled therapy for chronic and acute lung diseases.

2.2 ECM Nanoparticles

To combat lung injury from ARDS, mechanical ventilation, and VAP, our solution is to develop nanoparticles from the extracellular matrix (ECM) of mouse mesenchymal stromal cells (MMSCs) that can stimulate tissue healing and prevent bacterial infection.

2.2.1 Size Properties of Nanoparticles

The distal regions of the lungs are a difficult target to reach. The complex, narrowing, and angled airways can block the delivery of therapeutics and change the dynamics of airflow delivery (49). Deposition of the therapy on the airways can occur due to the mucus secretions and tubule branching. Time is another important aspect to consider, as deposited materials are cleared from the lungs 24 hours after entry due to mucociliary clearance and interactions with surfactant and proteolytic enzymes (50). Correct sizing of nanoparticles may help the treatment avoid obstacles and navigate through the branching airways of the lungs. Size also influences the pathways in which nanoparticles undergo cellular uptake. Nanoparticles in the range of 120-150 nm enter using clathrin or caveolin-medicate endocytosis. Larger particles, in the range of 2-3 μm may enter via phagocytosis (51).

A patient with ARDS, VAP, or receiving mechanical ventilation therapy even has a quality of ventilation and higher mucus production due to the inflamed state of the lung (52). An immune response will also recruit more alveolar macrophages to the injured lung, which will increase the chance the treatment will be engulfed (50). Particle size is a factor in bacteria cell uptake as well, the smaller the particle, the greater the antimicrobial effect. It was found that

silver nanoparticles were able to completely inhibit bacterial growth at a size of 10 nm. Particles sized at approximately 90 nm were found to effectively inhibit bacteria as well, just at a higher concentration (53). To reach the distal regions of the lungs and help avoid obstacles from inflammation, our goal is to create nanoparticles sized within the range of 50-260 nm nanoparticles.

2.2.2. Charge Properties of Nanoparticles

The surface charge influences the ability of the nanoparticles to avoid deposition in mucus, cellular uptake, and cytotoxicity (50). Mucosal fluid is known to possess a net negative charge, due to its composition of carboxyl groups of sialic acid and carbohydrate-bound ester sulfate residues (54). To repel mucus secretions in the inflamed airways, nanoparticles should have a negative surface charge (53). The charge is also an important factor to prevent the aggregation of nanoparticles in the lung. Nanoparticles need to have enough charge density to avoid accumulation in one part of the airway, or else the delivery of the particles will be inhibited and destroyed by the immune defenses (55).

Surface charge influences cellular uptake, as positively charged particles are known to enhance the internalization of non-phagocytic cells compared to neutral charge then negatively charged particles respectively. However, phagocytic cells also favored the uptake of positively charged particles. It may be beneficial to have a slightly more negative charge in the sensitive and inflammatory lung environment to help the nanoparticles evade destruction via phagocytosis (56). The surface charge of nanoparticles affects the cytotoxicity as well, as positively charged particles are known to be more cytotoxic, as the positive charge can induce cell necrosis, disrupt the cell membrane, and increase hemolysis upon entering the bloodstream (51,57).

In regard to bacterial cells, positively charged nanoparticles were shown to have an attraction towards the negatively charged bacteria cell wall, leading to the positively charged particles being more effective at inhibiting bacterial growth (58). Considering all of these factors, our goal was to develop nanoparticles at a slightly negative charge to lower cytotoxicity, prevent immune cell uptake, and prevent aggregation of nanoparticles in mucosal secretion.

2.2.3. Pig Lung ECM Nanoparticles

Previously, ECM from pig lungs has been harvested and developed into a nanoparticle treatment. Using sodium deoxycholate and triton-X solutions as detergents, the ECM was extracted, lyophilized, and digested with acetic acid. Electrospray deposition was then used to create ECM nanoparticles. It was determined that the pig lung (PL) nanoparticles were not cytotoxic and increased the cellular proliferation of alveolar epithelial cells. The PL nanoparticles were also able to modulate a pro-regenerative phenotype macrophage after introduction to murine bone marrow-derived monocytes. Nanoparticles were chosen as the method of delivery for our MMSC ECM for both their size and charge characteristics as well as previous success with PL ECM nanoparticles (59).

3. Extracellular Matrix (ECM)

The ECM is a three-dimensional scaffold that serves to allow cellular attachment and communication while regulating several processes for cell homeostasis including cell proliferation, differentiation, and migration (60). Fibroblast cells are mainly recognized as the source of ECM protein fibers to form the interconnecting network during wound repair and tissue regeneration (61). Protein components are either involved in the structural integrity of the tissue or involved in cellular signaling. Collagen, elastin, and fibronectin function to allow for

cell adhesion and tissue integrity, while growth factors and matrix metalloproteinases (MMPs) are involved in initiating processes such as wound healing (60).

The ECM structure can be divided into two different sections, the basement membrane, and the interstitial matrix. The basement membrane portion of the ECM is located in between the endothelial and epithelial cells (62). The main function of the basement membrane area in the matrix is to provide structure for epithelial and endothelial layers through integrin binding and regulate the proliferation, differentiation, and migration of cells through the binding of cell surface receptors to cytokines (63). The interstitial matrix surrounds the basement membrane. The interstitial space is composed of the three-dimensional interconnecting protein network, which provides a protective layer against any forces or injuries (64). Fibroblast cells are also located within the interstitial matrix (65). This area of the matrix is considered to be an active environment, as cytokines are released into the matrix to interact with surrounding cells (60).

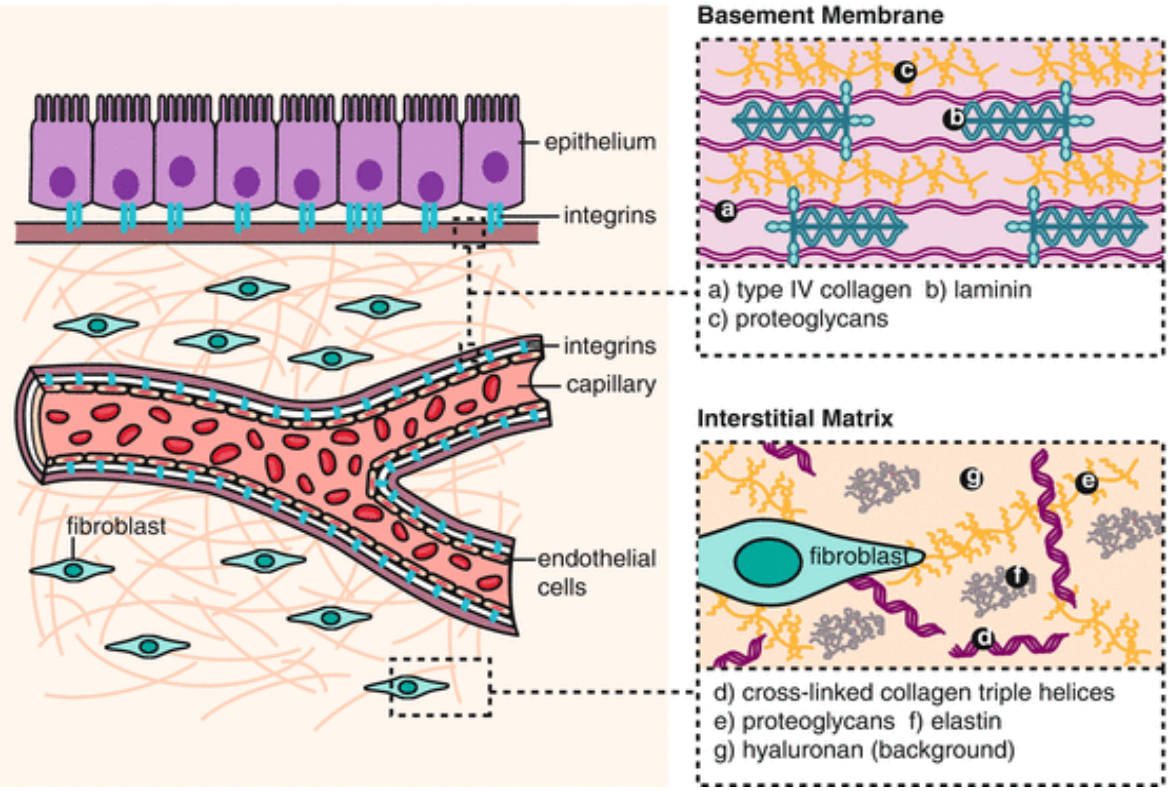

Figure 4. Division of the Basement Membrane and Interstitial Layers of the ECM (65).

Different tissues will have varying ECM components depending on their function and structure (61). ECM of the lung is composed of collagens, proteoglycans (perlecan, versican), glycosaminoglycans (heparin and hyaluronic acid), elastin fibers, laminins, fibronectin (66,67). The ECM is classified into two structures in lung tissue: the basement membrane and the lung parenchyma, mainly composed of collagen and elastin that can provide structural integrity during the inhalation of air (68).

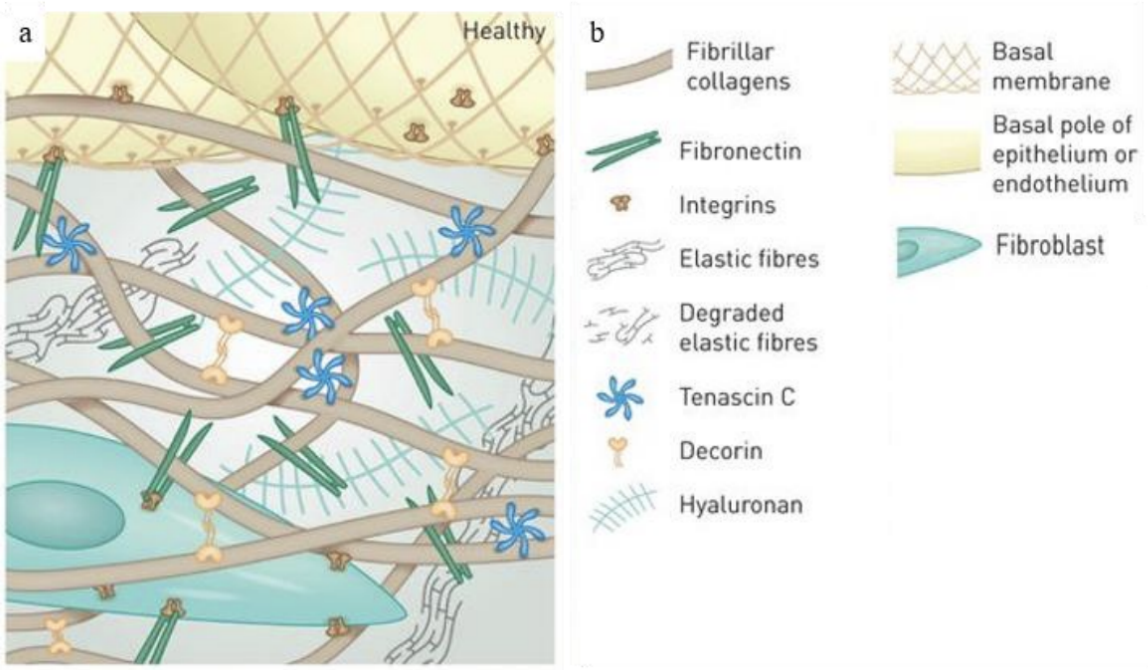

Figure 5. a) Figure of ECM structure and components in healthy lung tissue. b) Key of ECM components (69).

3.1.MSC ECM and Decellularization Processes

The ECM of MSCs is classified as a component of the MSC secretome. The MSC secretome has been characterized to contain soluble bioactive molecules that stimulate a desirable regenerative tissue response (70). To obtain the ECM of MSCs, decellularization processes can be utilized (71). Essentially, decellularization involves removing the cellular components of tissue to obtain the protein scaffold network (72). Because the ECM can be harvested in its natural structure, it can retain its important biological properties, such as regulating cellular proliferation, migration, and differentiation (73). Another property of the ECM that makes it a desirable biomaterial is that it is biocompatible, as once solubilized the

ECM can be degraded in the body and release growth factors that can stimulate the process of tissue repair.

Decellularized ECM is also able to elicit a smaller-scale immune response in comparison to other materials. After an initial inflammatory response to the material involving both neutrophils and inflammatory cytokines, the innate immune response shifts to a wound repair response around 48 hours later. Recruited macrophages shift to a wound-healing phenotype and cells begin to degrade the decellularized ECM into repaired functional tissue (74).

Various methods can be included in a decellularization protocol, including using chemicals and detergents, enzymes, physical forces, such as thermal shock and electroporation, or a combination of several techniques (74,75). In order for a tissue to be considered successfully decellularized, cells and genetic material must be depleted from the source tissue. The goal for the depletion of genetic material in decellularized ECM materials is to have less than 50 ng of double-stranded DNA per mg ECM dry weight, contain DNA fragments that have less than 200 base pairs, and possess no visible nuclear material. The decellularization process should also have a high efficacy of retaining important ECM proteins, including collagen, glycosaminoglycans (GAGs), fibronectin, laminin, and growth factors (72).

3.2 Key ECM Structural Components: Collagen, Elastin, and Fibronectin

Collagen is the most abundant fibrous protein, as it constitutes 30% of the ECM proteasome (67). The main purpose of collagen is to provide structure, and strength, and regulate cellular attachments for the matrix (64). Fibroblasts are the main source of collagen, organizing the fibrils into sheets that align to form the three-dimensional structure of the ECM (77). Collagens are classified into different types based on the morphology of their molecular structure alpha-chains (67). Collagens I, II, and III have been described to make up most of the collagen

content in the ECM, as 80-90% of the ECM collagens consist of those types. Type I-III collagens all contribute to the fibril network that promotes tissue integrity, while collagen IV is the main collagen found in the basement membrane (60, 77).

Another protein that is critical to the structural integrity of the ECM is elastin (64). Collagen and elastin are both components of the mesh interworking network of the ECM. The monomer tropoelastin forms the cross-linked elastin polymer, generating elastic fibers during synthesis. Elastin is a key ECM component of tissues that undergo deformation, such as the skin, arteries, heart valves, lungs, and ligaments (78).

The glycoprotein fibronectin is another fibrillar protein within the ECM network. The main role of fibronectin is to organize the ECM structure and mediate the attachment of cells to the ECM. Fibronectin can bind to itself as well as collagen, which helps to organize the interstitial space of the ECM (62). Additionally, fibronectin can bind to cell-surface receptors, and heparin, a glycosaminoglycan that promotes cell adhesion and ECM production (79). If an injury occurs to an epithelial barrier, fibronectin promotes platelet formation on the wound and recruits neutrophils, monocytes, fibroblasts, and endothelial cells to the injury site to help stimulate the restoration of the epithelial layer (80).

3.3 Key ECM Components: Glycosaminoglycans

GAGs are large polysaccharides that contain amino sugar or uronic acid. Molecules that are classified as GAGs include hyaluronan, chondroitin, dermatan sulfate, heparin, and keratin (81). GAGs can be attached to a core protein to be considered a proteoglycan. Examples of proteoglycans in the ECM include hyaluronan, perlecan, decorin, and laminins. Hyaluronan provides hydration to the tissue as well as serves as a part of the compressive barrier to external forces. Perlecan and decorin are able to retain growth factors in the ECM (67). Laminins are the

most abundant glycoprotein in the basement membrane portion of the ECM, where they serve as binding sites for epithelial cells as well as organizing the collagen fibrils in the basement membrane (62).

3.4 Key ECM Components: Growth Factors

Growth factors are capable of stimulating tissue regeneration through cellular proliferation, differentiation, and migration and there are several ways in which they interact with the ECM. The ECM is capable of both interacting with growth factors to issue a cellular response and storing growth factors (82). Vascular endothelial growth factor, fibroblast growth factor, and TGF-β are all growth factors that can interact with the ECM to exhibit a wound-healing response (83). When binding to the ECM, these growth factors will attach through the heparan or heparan sulfate (60). If the ECM encounters the proteases and matrix metalloproteinases, the growth factors embedded in the ECM can be released into the environment to initiate a cellular response (84).

3.5 Key ECM Components: Antibacterial and Bioactive Peptides

Another component of the ECM is small amino acid sequences, usually consisting of 2-50 amino acids, labeled as antimicrobial peptides (AMPs). AMPs can exhibit antimicrobial properties or increase the synthesis of ECM proteins (85). Upon degradation of the ECM through tissue injury, peptides can bind to integrins, and growth factor receptors, and modulate inflammatory cells (86). Some of these bioactive peptides have been identified, including tumstastin, derived from collagen IV, which can increase fibroblast migration and proliferation, and peptide DGGRYY, from collagen I, which activates neutrophils. Other peptides have not been identified by name, such as peptide fragments from elastin, which are able to encourage fibroblast migration (87). Peptides formed from degraded fibronectin, laminin, and vitronectin

have been proven to have antimicrobial activity against both gram-positive *S. aureus* and gram-negative *Escherichia coli* and *P. aeruginosa* (88).

4. Mesenchymal Stromal Cells

The utilization of mesenchymal stromal cells (MSCs) in tissue repair applications is prevalent due to their capability for self-renewal and differentiation into adipocytes, chondrocytes, and osteocytes. MSCs are sourced from bone marrow most commonly, but they also can be derived from adipose tissue, the umbilical cord, and the placenta (89). Typically, MSCs are released during an inflammatory response to help heal a site of injury. Once they migrate to the injury site, MSCs are able to secrete growth factors, anti-inflammatory cytokines, and upregulate the production of ECM to modulate the immune response to repair tissue damage (90). MSCs are our choice of source material for ECM due to their secretome, healing abilities, and ability to polarize macrophages.

4.1 Mesenchymal Stromal Cell Secretome

The MSC secretome consists all of the molecules released by a cell, including cytokines, mRNAs, extracellular vesicles, growth factors, and lipid molecules (91). The utilization of the MSC secretome for treatment is beneficial as it is a cell-free biomaterial, lowering the risk of rejection by the immune system (92). These molecules can impact cell-cell signaling by inducing a physiological response, including stimulating the production of ECM, suppressing apoptosis, and activating anti-fibrotic, anti-inflammatory, or angiogenic responses (93). In vitro studies have shown that the secretome can affect several different types of both innate and adaptive immune cells, including macrophages, neutrophils, and T and B lymphocytes (94). MSCs have been proven to secrete programmed death-ligand (PD-L1), which inhibits T cell activation and upregulates T cell apoptosis. Additionally, to suppress a pro-inflammatory response, the secreted

cytokines prostaglandin E2, TBF-B1, and IL-6 all inhibit the function of T cells, macrophages, and neutrophils (93). It is important to note that the secretome differs depending on the origin of the MSCs. The secretome of bone-marrow derived MSCs has been shown to increase gene expression to encourage re-epithelialization in human skin models, while the secretome from adipose-derived MSCs has demonstrated abilities to induce fibroblast migration to the injury site to increase wound-healing rate (94). MSC secretome is known to contain AMPs. These AMPs can inhibit the growth of bacteria through depolarization of the bacterial cell membrane and slow the formation of the protective biofilm layer for *P. aeruginosa* and *S. aureus* (95). All of these factors make the MSC secretome a viable candidate as a biomaterial for nanoparticles.

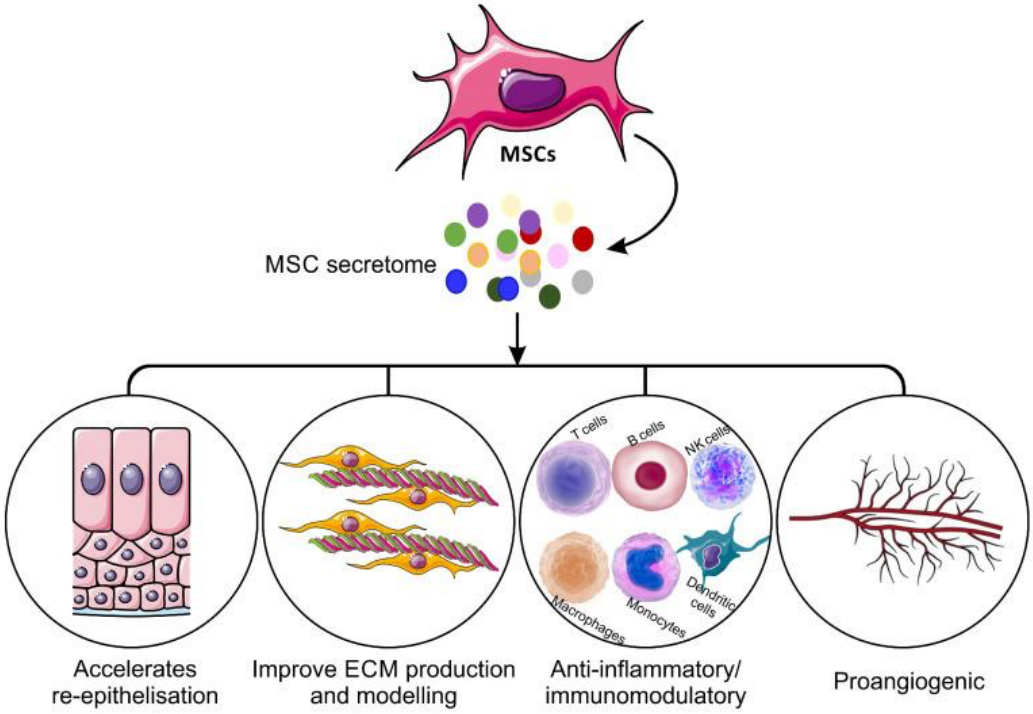

Figure 6. The pro-regenerative abilities of the MSC secretome (91).

4.2 Healing Abilities

MSCs have a renowned ability to promote cellular proliferation and wound healing at an injury site in various cell types. Treatment of MSCs increases the recruitment of fibroblasts to an injury. With more fibroblasts recruited, more ECM will be deposited to promote tissue regeneration. In a mice model of ALI, it was proven that MSC treatment decreased the effects of liposaccharide induced injury by lowering the expression of pro-inflammatory cytokines, IL-6, and interferon-γ, neutrophil recruitment, and prevented the thickening of the alveolar walls (96). MSCs also secrete paracrine factors to protect alveolar epithelial cells from destruction when a pro-inflammatory environment is stimulated in the lungs. The secretion of paracrine keratinocyte growth factor (KGF) from bone-marrow derived MSCs is responsible for this effect, as KGF allows the Na^+ channels to continue transport, preventing pulmonary edema and preserving type II alveolar epithelial cells (97). Additionally, MSCs have displayed the potential to mediate the effects of ARDS by preserving the alveolar epithelial barrier and increasing the clearance of alveolar fluid in the inflamed lung. In fact, the administration of MSCs as a therapy in human ARDs patients improves patient survival rates due to the anti-inflammatory, tissue repair, and antimicrobial properties of the MSCs (98).

4.3 Polarization of Macrophages

Along with regulating the immune response, MSCs have the ability to increase the presence of M2 phenotype macrophages through modulation. Traditionally, M1 phenotype macrophages have been defined as macrophages that inhibit cellular proliferation, clear pathogens, and issue an immune response while macrophages that promote wound healing and tissue repair are classified as the M2 phenotype (99). At the start of the injury in the exudative phase of ARDS, alveolar macrophages are modulated into the M1 phenotype, which secretes

TNF-α, IL-1, and reactive oxygen species that culminate into an inflammatory response (100). The addition of MSCs to an injured tissue can modulate the alveolar macrophages into the wound healing M2 phenotype. It is believed that the secretome of MSCs is the mechanism behind the modulation of macrophages to the M2 phenotype. MSCs can mediate the production of prostaglandin E2, which can polarize M2 macrophages (101). Transforming growth factor-beta, a growth factor known to decrease inflammation, can induce the change in macrophage phenotype from M1 to M2 while preventing excessive inflammation (102). A chemokine that is recognized for its ability to recruit macrophages and monocytes during angiogenesis, CCL2 can convert M1 macrophages to the M2 phenotype (103). These are just a few examples of molecules in the MSC secretome that are able to regulate the role of macrophages released during an immune response.

Research Design

Rationale

Our goal is to harness the regenerative and antimicrobial properties of the MMSC ECM into the size of a nanoparticle that can reach the distal region of the lung. ECM proteins including collagen, glycosaminoglycans, and growth factors increase cellular proliferation without eliciting an immune response. The MSC secretome releases cytokines and peptides that activate the proliferation of progenitor stem cells, stimulate the formation of new ECM, suppress apoptosis and fibrosis, and inhibit bacterial growth (93, 96). The nanoparticle size will allow the treatment to reach the distal region of the lungs. The negative zeta potential of the nanoparticles will avoid the deposition of mucus in the lung epithelial barrier (59).

Hypothesis

We hypothesize that the sizing of the nanoparticles and pro-regenerative effects of the MMSC ECM will combine and form a treatment that can reach the distal region of the lungs and stimulate lung tissue growth after injury. To evaluate this hypothesis, MMSC ECM was obtained through decellularization and fabricated into nanoparticles using electrospray deposition. The effectiveness of the decellularization process was evaluated by determining the concentration of key ECM proteins, collagen, and glycosaminoglycans, as well as calculating the lowering of DNA concentration. The nanoparticles were characterized by evaluating the size and zeta potential. *In vitro* testing using mammalian cell lines was used to determine the cytotoxicity and wound healing abilities of the nanoparticles. Bacterial cell cultures were grown to assess the antimicrobial activity of the ECM nanoparticles.

Specific Aims

Aim 1. Optimize the procedure for obtaining extracellular matrix from mouse mesenchymal stromal cells. Ensure the procedure retains key structural components of the ECM while reducing DNA concentration.

Aim 2. Optimize the electrospray deposition process to create the MMSC ECM nanoparticles. Fabricate the nanoparticles with a size and zeta potential that will allow for administration into the distal regions of the lungs. Use mass spectrometry to analyze the proteins in both the MMSC ECM nanoparticles and PL ECM nanoparticles.

Aim 3. Evaluate the biocompatibility of the MMSC ECM nanoparticles with mouse lung epithelial cells and mouse mesenchymal stromal cells. Then evaluate the wound-healing effects of the MMSC ECM nanoparticles with human lung fibroblasts.

Aim 4. Evaluate the antimicrobial properties of the MMSC ECM and PL ECM nanoparticles against common lung pathogens, *Escherichia coli*, *Staphylococcus aureus*, and *Pseudomonas aeruginosa*.

Aim I

Methods and Materials

Mammalian Cell Culture and Medium Preparation

A cell line of mouse bone marrow derived mesenchymal stromal cells (MMSCs, Gibco) was grown on cell culture flasks (T75 and T175, Greiner) to obtain decellularized ECM (dECM). MMSCs were cultured in Dulbecco's Modified Eagle Medium (DMEM) modified with GlutaMAX supplement (Gibco). Media was supplemented with 10% fetal bovine serum qualified for mesenchymal stromal cells (FBS, Hyclone) and 250 µl of Gentamicin (Gibco). Cell culture conditions were set at an atmosphere of 5% CO2 at 37 ℃. The culture medium was changed every 2-3 days.

Mouse Lung Epithelial (MLE-12, ATCC) cells were grown in Dulbecco's Modified Eagle (Gibco) and supplemented with 2.5 mL of 100 mM sodium pyruvate (Sigma Life Sciences), 0.6 g of sodium bicarbonate (Flinn Scientific), 250 µL of 10 mg/mL insulin (Gemini Bio-Products), 5 mg of transferrin (Sigma-Aldrich), 5.2 µL of 0.5 mg/mL sodium selenite (Lonza), 50uL of 100 µM hydrocortisone (Lonza), 50 µL of 100 µM β-estradiol (Lonza), 5mL of 200 mM L-glutamine (Quality Biological), and 10 mL of FBS (Gibco).

Human fibroblast cells (NHLF, Lonza) were cultured using fibroblast basal medium (FBM, Lonza) with a growth supplement package (FGM2 SingleQuots, Lonza).

Decellularization with 0.1% Sodium Deoxycholate and DNase I

MMSCs were seeded on tissue culture flasks at a density of 500,000 cells for a T75 flask and two million cells for a T175 flask. Cells were cultured until 90-95% confluency, which was typically three-five days after initial cell seeding. The MMSC cell layer was washed five times

with 1X phosphate-buffered saline (PBS). A solution of 0.1% sodium deoxycholate was added to the cell flask and incubated for three minutes at 37 ℃. The ECM sheet was then collected and washed with Hank's Balanced Salt Solution (HBSS) three times. Tissue was centrifuged at 300 rcf for 2 minutes to remove the wash solution as needed if tissue was difficult to collect. The ECM tissue was submerged in a solution of DNase I (50 U/mL) and incubated at 37 ℃ for 30 minutes. DNase I solution was then removed and the dECM was washed with PBS three more times, centrifuging at 300 rcf for two minutes to collect supernatant if needed. dECM can be stored for up to 4 months at 4℃ in 2 mL of PBS and 2 mL of Antibiotic-Antimycotic Solution (100 U/mL Penicillin, 100 µg/mL Streptomycin, 0.25 µg/mL Fungizone, Thermofisher Scientific) (104). Before nanoparticle fabrication, the decellularized ECM tissue was lyophilized into a powder. The powder was formed after a lyophilization cycle of 36 hours and then stored at -20℃ for long-term storage.

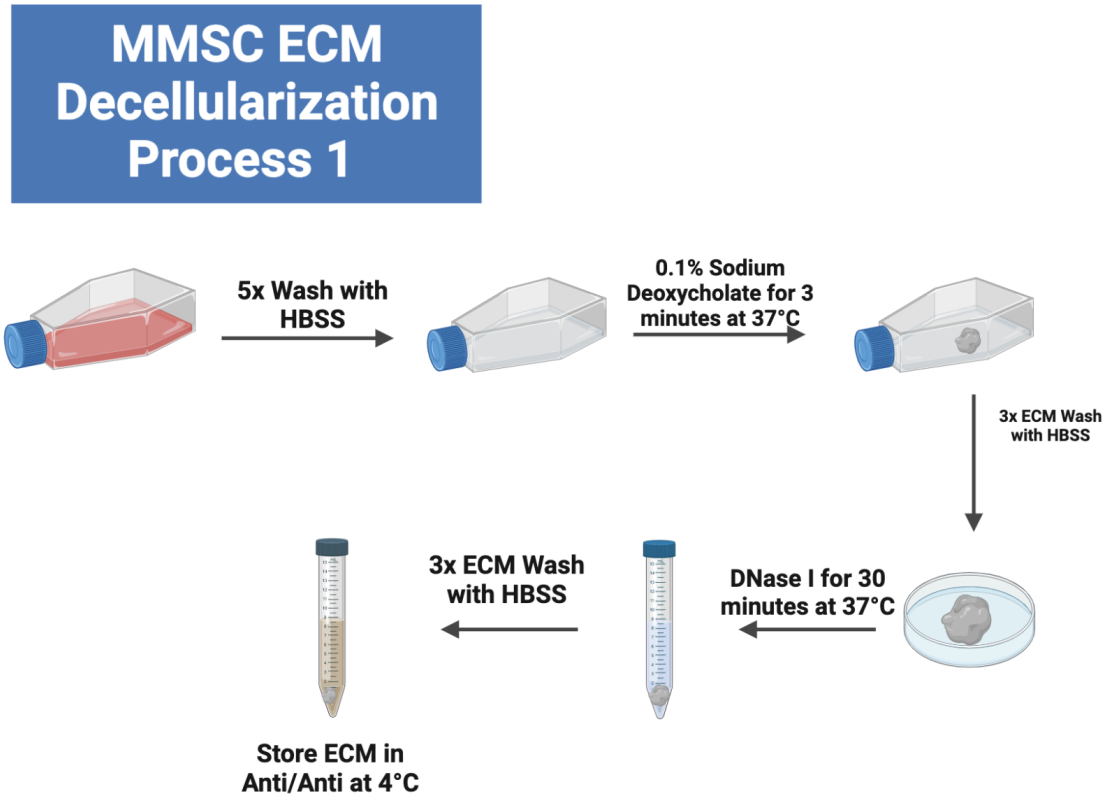

Figure 7. Decellularization with 0.1% Sodium Deoxycholate.

Decellularization with 0.5% Triton-X

MMSCs were seeded on tissue culture flasks at a density of 500,000 cells for a T75 flask and two million cells for a T175 flask. Cells were cultured until 90-95% confluency, which was typically three-five days after initial cell seeding. The MMSC cell sheet was washed with PBS five times. A solution of 0.5% TritonX-100 (Triton-X) containing 20 mM of NH_4OH in PBS was added to the flask and allowed to incubate at 37°C for 5 minutes. The ECM sheet was treated with a solution of DNase I (100 U/mL) then incubated for 1 hour at 37°C. The dECM was removed from the flask and washed with PBS three times. The dECM tissue was stored in a solution of 2 mL of PBS and 2 mL of Antibiotic-Antimycotic Solution (Anti/Anti) (100 U/mL

Penicillin, 100 µg/mL Streptomycin, 0.25 µg/mL Fungizone, Thermofisher Scientific) at 4°C for up to 4 months (105).

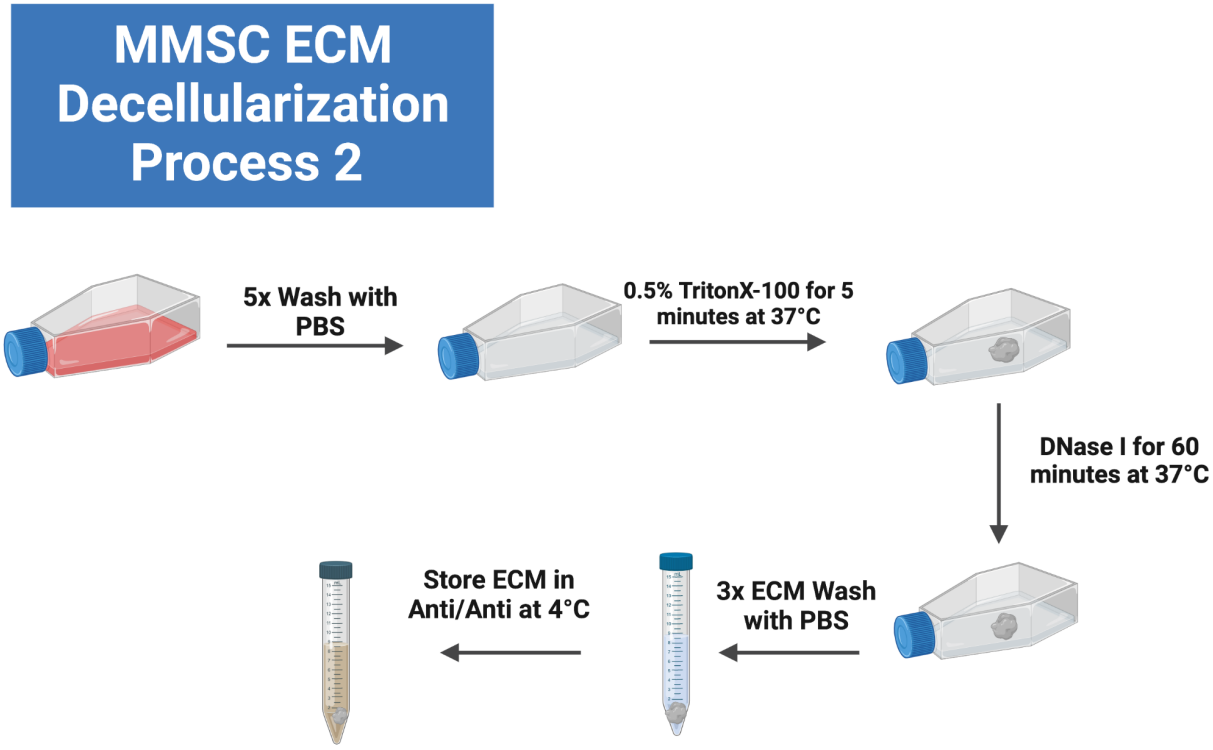

Figure 8. MMSC ECM Decellularization with 0.5% Triton-X.

Evaluation and Quantification of Decellularization Procedures

Protein and DNA quantification assays were performed to determine the effectiveness of each procedure in retaining critical protein content in the ECM and reducing the concentration of DNA in each tissue.

Sircol Collagen Assay

The sircol soluble collagen assay kit (Biocolor, Ltd) was performed on an untreated MMSC sheet and dECM treatment with 0.1% sodium deoxycholate + DNase I or 0.5% Triton-X + DNase I to evaluate the preservation of collagen in the dECM. Before starting the assay protocol, MMSC sheets and dECM tissue samples were digested with a solution of 0.5M acetic acid with 0.1 mg/mL pepsin overnight at 4℃. The manufacturer's collagen isolation and concentration protocol were both followed before proceeding with the general protocol.

Blyscan Glycosaminoglycan Assay

The glycosaminoglycan blyscan assay kit was utilized to find the concentration of glycosaminoglycan proteins, in both dECM treated with sodium deoxycholate and triton-X then compared to an untreated MMSC sheet. dECM tissue samples and MMSC sheets were digested with papain extraction reagent for 3 hours at 65℃. Then the assay protocol was followed.

Picogreen Assay

The concentration of DNA in each tissue was quantified using the picogreen assay kit (Invitrogen, Thermofisher) and compared to an MMSC sheet. dECM tissues were digested overnight at 65℃ with 1 mL of papain digestion solution following the manufacturer's instructions. Samples were diluted 5 times in 1X TE buffer solution. To obtain initial the DNA

concentration of the MMSCs before decellularization, the MMSC sheet was allowed to reach 90% confluency and then treated with TRIzol for 10 minutes at 25℃ to extract DNA. Samples were diluted 5 times in 1x TE buffer solution and the assay was performed following the manufacturer's protocol.

Statistical Analysis

All statistical analyses were performed using Prism 9 (GraphPad). Ordinary analyses of variance with multiple comparisons were used to determine the significance of the results. Significant results were determined to have a p-value < 0.05.

Results

Evaluation of Decellularization Procedures

Sircol Collagen Assay

After the MMSCs were 80-90% confluent, we extracted and determined the amount of collagen contained within the ECM sheet. The ECM was determined to contain 170.0 ng/cm^2 of soluble collagen after treatment with 0.1 mg/mL of pepsin in acetic acid. These baseline results were then compared to the triton-X and sodium deoxycholate protocols that were performed to determine which retained more soluble collagens in the harvested ECM. The procedure using triton-X had a soluble collagen concentration of 6.12 ng/cm^2, while the ECM obtained using sodium deoxycholate was 2.96 ng/cm^2.

Blyscan Glycosaminoglycan Assay

Similarly, to the sircol collagen assay, GAG content of the ECM obtained from the triton-100 and sodium deoxycholate procedures was compared to each other and to a baseline of cells. Before decellularization, it was determined that the ECM contained 4.846 ng/cm^2 of GAGs using

a papain extraction regent recipe provided by the manufacturer. The triton-X method retained 4.6 ng/cm^2 of GAGs which was greater than the concentration of GAGs retained by the sodium deoxycholate method which was determined to be 0.35 ng/cm^2.

Picogreen Assay

The picogreen assay was performed to determine how effective the DNase I incubation step was in each protocol. A confluent cell layer of MMSCs was calculated to have 90.71 ng/mL of DNA by extracting DNA with TriZol. This baseline number was then compared to the different decellularization procedures, with the goal to consistently obtain ECM with a DNA concentration less than 50 ng/cm^2. Using tritonX-100 + DNase I, ECM was harvested with 14.129 ng/cm^2 of DNA. Additionally, both sodium deoxycholate alone and sodium deoxycholate + DNase I were tested. Sodium deoxycholate alone was reported to have a DNA concentration of 13.25 ng/cm^2. When DNase I was included in the sodium deoxycholate protocol, the ECM had a DNA concentration of 5.15 ng/cm^2.

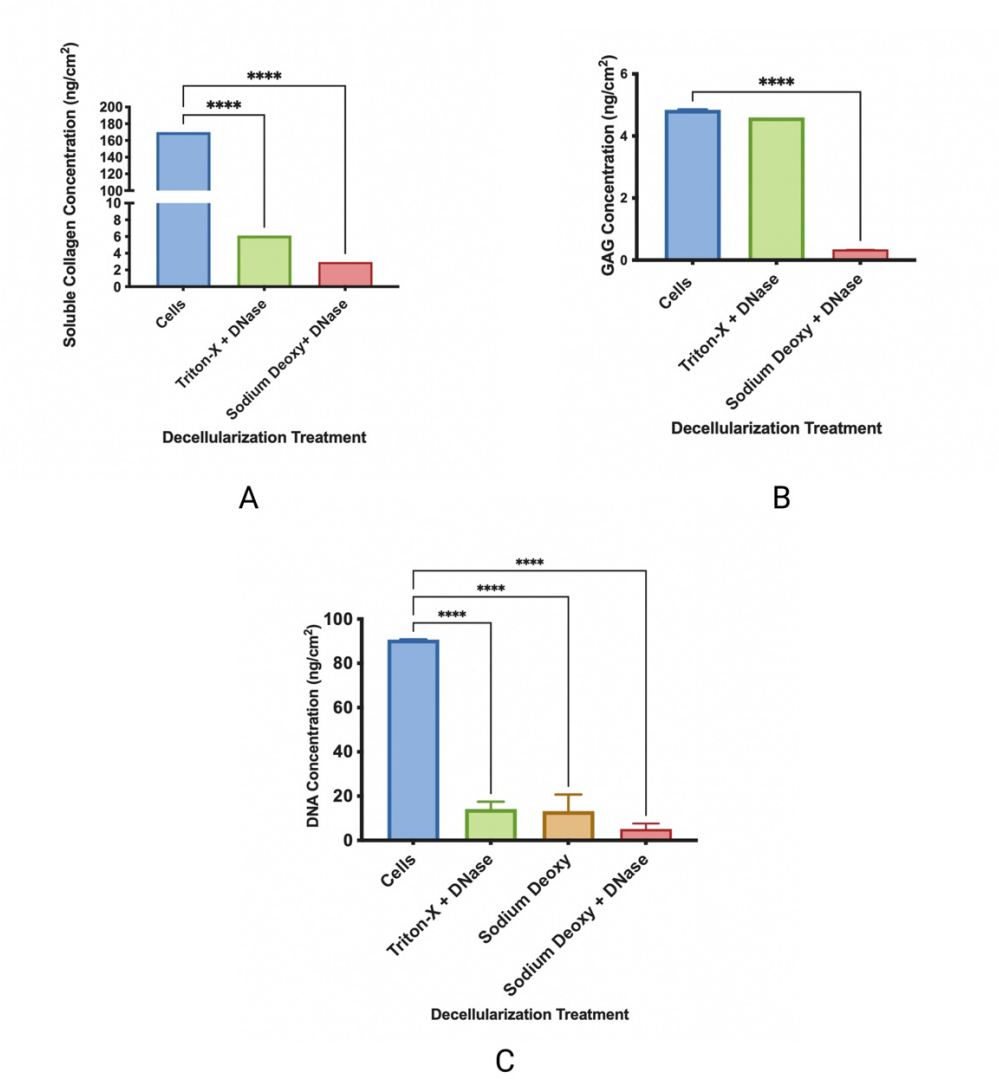

Figure 9. Difference in Concentration ECM Components based on Decellularization Procedure. A) Concentration of Soluble Collagen (ng/cm^2); B) Concentration of GAGs (ng/cm^2) C) Concentration of DNA (ng/cm^2). Data is displayed as the mean± standard deviation. * indicates $p< 0.05$, ** indicates $p<0.001$, *** indicates $p<0.0001$. Cells N= 3, Triton-X + DNase N=1, Sodium Deoxy N=3, Sodium Deoxy + DNase N=3.

Discussion

For both the triton-X and sodium deoxycholate procedures, it was proven that important structural ECM proteins collagen and GAGs were retained in the dECM. The triton-X method was able to preserve a larger concentration of proteins. Similar to other literature procedures, the decellularization procedure utilized sodium deoxycholate had a lower ECM protein retention compared to when other detergents were utilized (104). This could be due to the fact that triton-X is a non-ionic detergent while sodium deoxycholate is classified as an ionic detergent. Non-ionic detergents are used to solubilize proteins by interfering with lipid-protein or lipid-lipid interactions, while ionic detergents can disrupt covalent bonds between proteins. For this reason, ionic detergents have the potential to damage and fragment GAGs, growth factors, and collagen compared to nonionic detergents (106). However, ionic detergents have been shown to be more effective at destroying nuclear material.

For the detection of nuclear material using the picogreen assay, we saw that the sodium deoxycholate + DNase combination was more effective at removing DNA from the MMSC ECM. Without DNase, sodium deoxycholate can cause the accumulation of DNA on the tissue surface (107). For this procedure, DNase was found to be an essential step in the protocol, as it decreases the amount of DNA in the dECM by approximately 40% when compared to using sodium deoxycholate alone. Several wash steps were also added to the protocol to ensure residual DNA fragments were removed from the dECM. Including DNase reduces the risk that the dECM will be cytotoxic and rejected by the immune system (107).

Ultimately, we decided to use the combination method of sodium deoxycholate + DNase I to extract the ECM from the MMSCs. The efficient reduction of the DNA concentration from this protocol was considered to be an important property to ensure the dECM would be biocompatible. Even though collagen and GAG content were reduced using sodium

deoxycholate, mass spectrometry would be used to confirm that the decellularization method still retained both proteins. Therefore, we chose the sodium deoxycholate method over the triton-X due to its ability to reduce cell DNA concentration.

Aim 2

Methods and Materials

MMSC Nanoparticle Fabrication using Electrospray Deposition

To create the MMSC ECM nanoparticles, a previous protocol was utilized from the Heise lab and optimized to form a stable electrospray cone. The stable cone during the electrospray deposition is critical to obtaining consistently sized and charged nanoparticles to prevent aggregation during the purification process. The protocol was altered by decreasing the working distance between the needle and stationary foil base for the spray from 10 cm to 8 cm. The working distance is an important factor in nanoparticle size (108). The applied voltage of the electric field was adjusted to -15 kV instead of -25 kV. The change in voltage helped prevent irregular particle size, which would help prevent the aggregation of nanoparticles during the purification process.

Decellularized MMSC ECM powder (50 mg) was dissolved in 80% V/V (volume/volume) of acetic acid and stirred for 48 hours at room temperature. Acetic acid was the solvent of choice as it can successfully dissolve the ECM powder without disrupting peptide bonds in the ECM proteins. After stirring, ECM-acetic acid solution was drawn up by a syringe with a 26 gauge blunt-tip needle. It is crucial a blunt-tip needle is used instead of a differently shaped needle, such as a tapered needle, or else the electrospray cone may be disrupted and misshapen. The needle was placed in a syringe pump and set to a flow rate of 0.6 mL/hour. Cables from the voltmeter were attached to the top of the 26 gauge needle and a piece of aluminum foil to complete the electrospray system. The voltmeter was set to -15 kV and a syringe pump was started.

Once the solution was deposited on the foil, the foil was sprayed with 70% ethanol and ECM nanoparticle residue was collected into a solution. The nanoparticles were shaped into the

correct size by drawing the solution through a series of needles, 18 gauge, 26 gauge, and then 27 gauge. The nanoparticle solution was then purified using a 0.45 um pore size filter. The nanoparticle solution was stored at -80℃ or lyophilized for 36 hours into a powder.

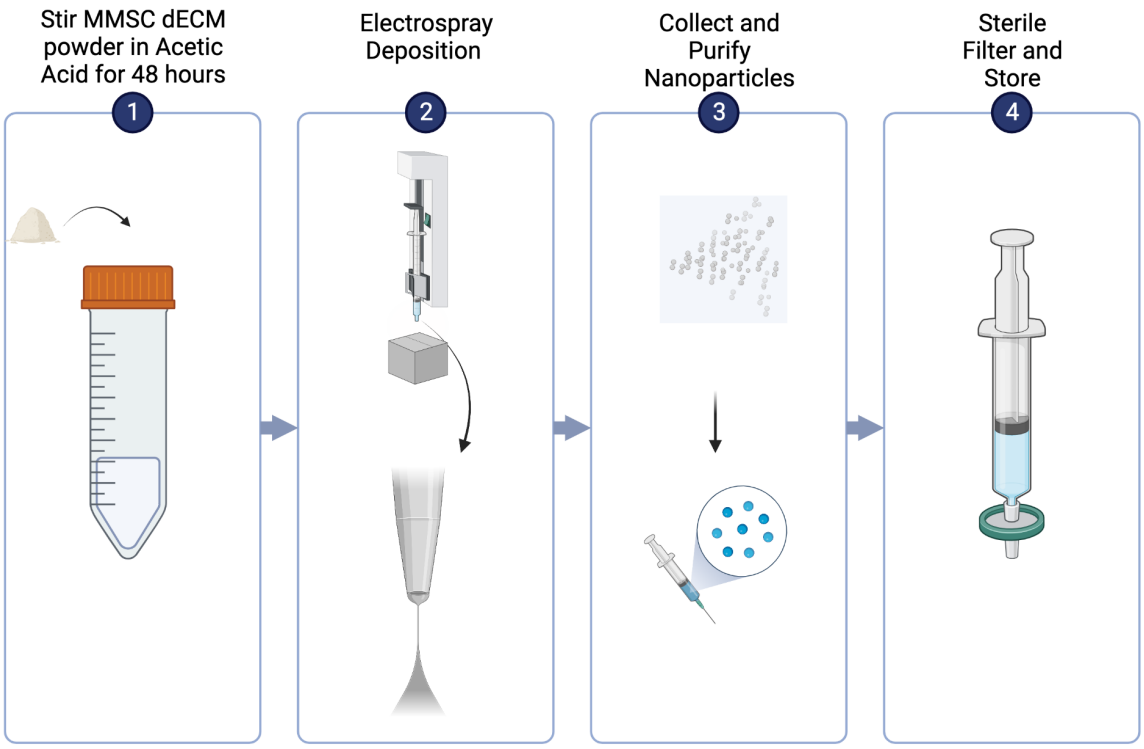

Figure 10. Electrospray Deposition Procedure.

Concentration of Nanoparticles in Solution

To determine the concentration of nanoparticles produced by electrospray deposition, the total volume of purified nanoparticle solution was recorded and then lyophilized. Once lyophilization was complete, the powder was weighed. The mass of the powder was divided by

the volume of the purified nanoparticle solution to obtain the concentration of nanoparticle stock for experimentation.

Scanning Electron Microscopy

The size of the MMSC ECM nanoparticles was determined using Scanning Electron Microscopy (SEM). A sample of aluminum foil containing the electrospray nanoparticles was affixed to a silicon wafer and coated with platinum to obtain the images.

A Malvern Zetasizer (ZN90) was utilized to obtain both the size and zeta potential of the MMSC ECM nanoparticles. One millimeter of the ECM nanoparticle solution (28.8% ethanol) was pipetted into a cuvette. Each sample was run 3 times for both size and zeta potential.

Mass Spectrometry

Mass spectrometry was completed with the assistance of the Biomolecular Analysis Facility at the University of Virginia. The lyophilized MMSC ECM nanoparticle and PL ECM nanoparticle samples were suspended in 1 mL of water (LC-MS grade) and 9 mL of cold methanol and 1 mL of cold acetone. The samples were allowed to precipitate overnight at -80℃ overnight. The next day, samples were centrifuged at 4℃ for 2 hours at 3,000 rpm. The pellets that were obtained were washed with 1 mL of cold methanol and followed by 20 minutes of centrifugation at 15,000 rpm for a total of three times. Protein pellets were dried and then suspended in 50 μL of 0.1 M ammonium bicarbonate and reduced using 10 mM dithiothreitol at room temperature for 1 hour. Then 50 mM iodoacetamide was added and incubated in the dark at room temperature for 30 minutes. The sample was then digested overnight at 37℃ with 0.5 μg of trypsin. For sample purification, C18 column tips were utilized then the samples were dried in a

speed vacuum and added to 0.1% of formic acid. 5 μL of each sample was injected to obtain the mass spectrum.

Scaffold 5 was used for mass spectrometry analysis. Peptide identifications were accepted if they could be established at greater than 95.0% probability and then proteins were sorted based on function, locality, and type of ECM protein. PeptideRanker was then used to determine if ECM proteins and peptides were potentially bioactive. Scores were on a scale of 0-1, with 1 being the highest probability of having bioactive properties (109).

Statistical Analysis

All statistical analyses were performed using Prism 9 (GraphPad). Ordinary analyses of variance with multiple comparisons were used to determine the significance of the results. Significant results were determined to have a p-value < 0.05.

Results

Size and Charge Characterization

After modification of the Heise electrospray protocol, the PL ECM nanoparticles were determined to have an average size of 200.6 nm (±6.3) and a zeta potential of -38.53 (±7.07). The MMSC ECM nanoparticles had an average size of 273.4 nm (±25.6) and a zeta potential of -11.17 (±0.611). As seen below, an image of the nanoparticles on the foil after electrospray deposition was obtained using SEM.

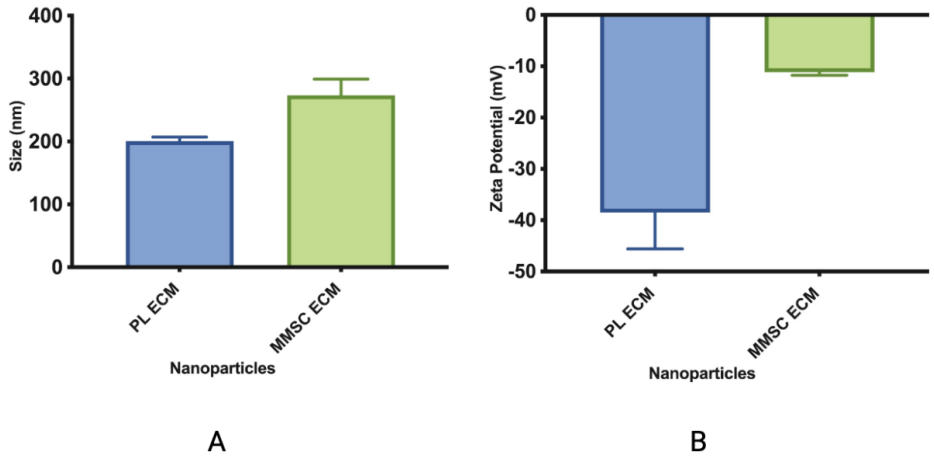

Figure 11. Size and Charge Comparison of the PL and MMSC ECM Nanoparticles. A) Size Comparison of the Nanoparticles. B) Zeta Potential Comparison of the Nanoparticles. Data displayed is the mean± standard deviation. N =3.

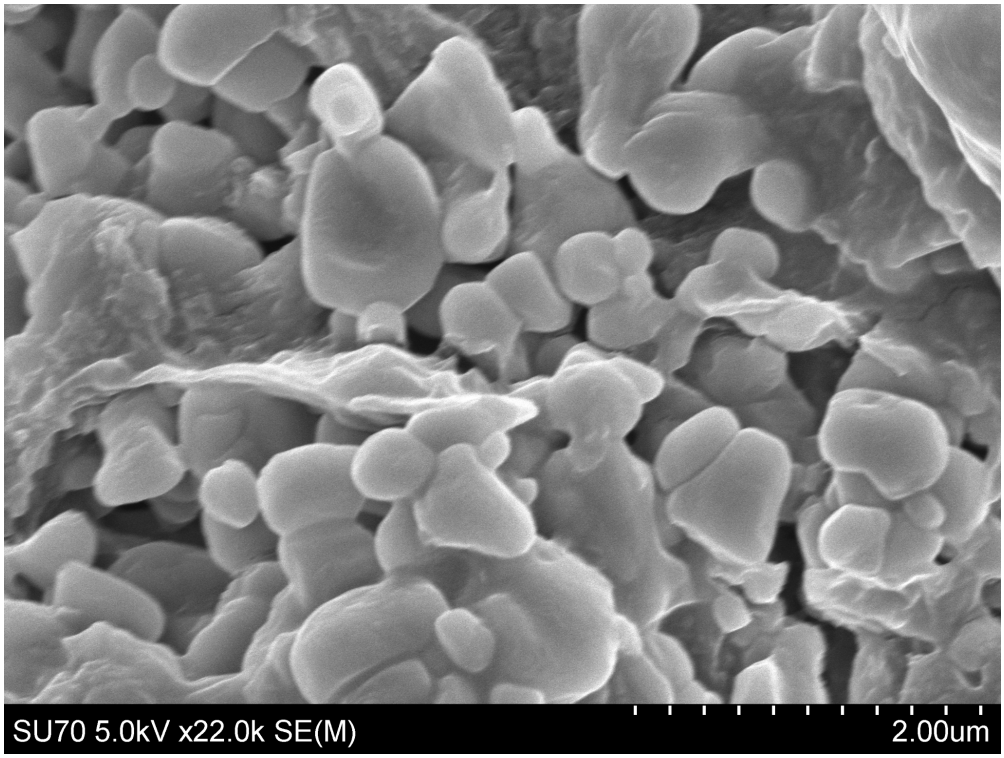

Figure 12. SEM Image of Deposited MMSC ECM Electrosprayed Nanoparticles on Aluminum Foil before purification.

Efficiency of Electrospray

Starting with 17 mL of nanoparticle solution for both the PL and MMSC ECM nanoparticles, it was calculated that the PL ECM nanoparticles were synthesized at a concentration of 0.064 mg/mL. The MMSC ECM had a concentration of 0.0411 mg/mL. During cell and bacterial testing, nanoparticles were added to either 10 mL of media or LB broth for starting concentrations of 6.4 ng/mL for PL ECM nanoparticles and 4.0 ng/mL for MMSC ECM nanoparticles. As both the PL and MMSC nanoparticle protocols begins with a concentration of 50 mg/mL of decellularized ECM in acetic acid, both materials had a similar deposition rate. The nanoparticle yield of the PL ECM nanoparticles was calculated to be 1.28% while the MMSC ECM nanoparticles were 0.82%.

Mass Spectrometry

The mass spectrometry results confirmed that both the MMSC and PL ECM nanoparticles contained important structural ECM proteins and potential peptides that contribute to their bioactivity. Both types of nanoparticles had the greatest percentage of proteins from the cytoplasm and then membrane-associated proteins. Scaffold 5 determined that 160 proteins from the total proteasome were from the ECM region in the MMSC ECM nanoparticles and 43 ECM proteins were in the PL ECM nanoparticles. Collagens, laminins, fibronectin, proteoglycans, glycoproteins, and growth factors were found in both nanoparticle samples. Integrins, keratin, and fibrillin were exclusive to the MMSC ECM nanoparticles. Elastin was only found in the PL ECM nanoparticles.

PeptideRanker indicated that the MMSC ECM nanoparticles were composed of several protein subunits that potentially could possess bioactivity, including peptide sequences derived from collagen, fibronectin, and laminin. In particular cationic sequences from fibronectin and the beta-1 chain of laminin are known to have antimicrobial effects (88). The membrane protein tetraspanin was found in the ECM proteins, which has been shown to have antimicrobial activity. Thrombospondin-1 and thrombospondin-2 were found as well. Hydrophobic regions from thrombospondins have been proven to have antimicrobial activity against both gram-positive and gram-negative bacteria (88). Glycoprotein fibulin-1 was found in the MMSC ECM nanoparticles known to encourage lung fibroblast proliferation and attachment (110).

In the PL ECM nanoparticles, a few peptides were discovered including Protegrin-4, a fragment from the cathelicidin class of proteins, which are known antimicrobial peptides (111). Azurocidin, a peptide that can inhibit the growth of gram-positive bacteria, was found (112). Acyl-CoA binding protein found in the PL ECM is similar to a known Acyl-CoA binding protein that has been proven to possess antimicrobial activity (113). Additionally, fragments from collagen, fibronectin, and laminin were identified in the PL ECM nanoparticles and rated as highly probable to be bioactive. Collagen type VI alpha 3 subunits have been identified to damage the extracellular membrane of *E. coli*, *S. aureus*, and *P. aeruginosa* (88). Cationic peptides from collagen type VI also contribute to the destruction of the bacterial membrane, as interactions occur with the highly negative charge of the bacterial membrane.

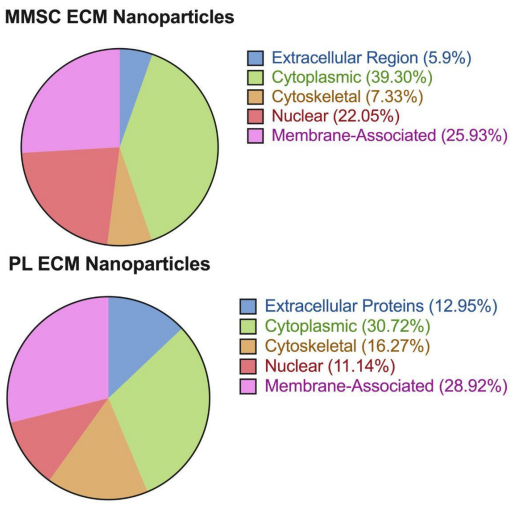

Figure 13. Analysis from Mass Spectrometry; Comparison of the location of proteins from the MMSC ECM Nanoparticles (top) and the PL ECM Nanoparticles (bottom).

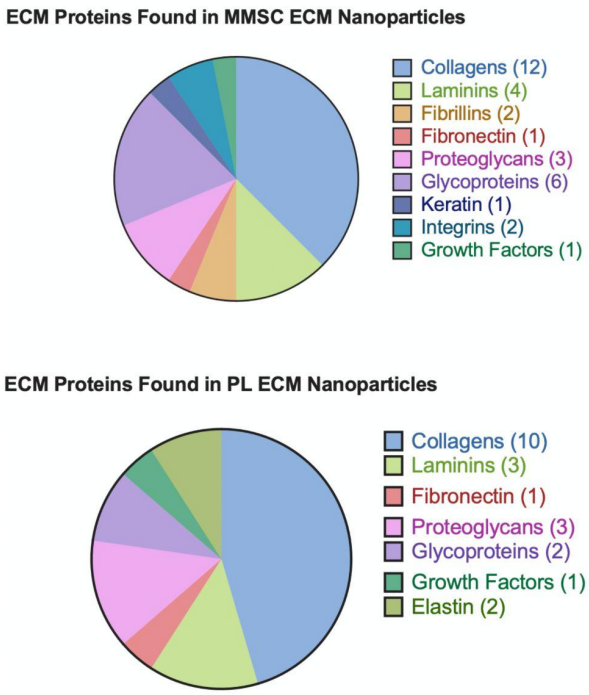

Figure 14. Categorization of Key ECM Proteins found in the MMSC ECM Nanoparticles (top) and the PL ECM Nanoparticles (bottom).

ECM Protein	PeptideRanker Bioactivity Score
Laminin subunit alpha-5	0.999916
Laminin subunit beta-1	0.999903
Laminin subunit gamma-1	0.999868
Thrombospondin-1	0.999425
Tetraspanin	0.997189
Thrombospondin-2	0.997116
Fibronectin	0.991198
Collagen alpha-1(XII) chain	0.991148
Collagen alpha-2 (IV) Chain	0.89322
Collagen alpha-2(I) chain	0.849786
Collagen alpha-1(I) chain	0.849393

Table 1. Selected MMSC ECM Nanoparticle Proteins and their predicted bioactivity ranking from PeptideRanker. Peptides are listed from the highest bioactivity score to the lowest.

ECM Protein	PeptideRanker Bioactivity Score
Laminin subunit alpha 3	0.999916
Laminin subunit gamma 1	0.999874
Collagen Type VI alpha 3	0.991472
Fibronectin	0.991215
Protegrin 4	0.902885
Azurocidin	0.88507
Collagen Type I alpha I chain	0.878195
Collagen Type VI alpha I chain	0.860133
Acyl-CoA binding protein	0.522456

Table 2. Selected PL ECM Nanoparticle Proteins and their predicted bioactivity ranking from PeptideRanker. Peptides are listed from the highest bioactivity score to the lowest.

Discussion

Size and Charge Characterization

MMSC ECM nanoparticles were found to have a similar size and charge as the PL ECM nanoparticles. In terms of size, both types of nanoparticles were smaller than 300 nm, meaning that they are capable of reaching the distal alveolar regions of the lungs (59). The SEM image shows that the purification step is critical for nanoparticle size and uniformity. Nanoparticles of different sizes and shapes are formed initially from the electrospray deposition, but through the use of needles and sonication, the nanoparticles can be purified to the size required to reach the distal alveoli.

Compared to PL ECM nanoparticles created in the past, which were established to be 225 nm (±67), the newly formed nanoparticles have a smaller standard deviation value. The size difference could be attributed to the revisions to the electrospray deposition protocol. The working distance between the needle tip and foil base was changed from 10 cm to 8 cm. Another modification was the applied voltage, which was decreased from -25 kV to -15 kV. Both of these factors contribute to affecting the jet cone of the electrospray and can cause irregularities in the size and shape of nanoparticles. A decrease in the working distance will increase the strength of the electric field, which will reduce the size of the nanoparticles and form a stable cone during electrospray. An ideal range for voltage was found to be -10 to -15 kV for chitosan nanoparticles. Outside of this range, nanoparticles had an irregular shape due to the instability of the jet cone (108). Based on our detected size and improved ease of nanoparticle purification, we can conclude that these modifications to the electrospray protocol improved the process.

The MMSC ECM nanoparticles had a lower zeta potential compared to the PL ECM nanoparticles produced with the revised electrospray method. Both of the ECM nanoparticles had a negative zeta potential, which may help prevent the aggregation of nanoparticles and

attachment to mucus once delivered to the lung (53, 55). The negative charge may help the nanoparticles evade detection by phagocytic cells and improve biocompatibility, which would be tested in the next aim.

Mass Spectrometry

Mass spectrometry results confirmed that characteristic ECM proteins were retained during the decellularization process with sodium deoxycholate and 80% acetic acid digestion for electrospray deposition. This is proven by the fact that collagens, laminins, fibronectin, glycoproteins, and growth factors were present in both samples. The PL ECM nanoparticles had a lower concentration of proteins categorized as ECM proteins compared to the MMSC ECM nanoparticles. This could be because the decellularization process for pig lungs is more intensive by using triton-X, sodium deoxycholate, and DNase I for longer incubation periods.

The MMSC ECM also had a more diverse proteasome including integrins, fibrillins, and keratins. The microfibrils in the ECM are composed of fibrillin, proving structural integrity and scaffolding for organ systems. Fibrillin is also critical in participating in the development of elastin fibrils (114). Keratin has been shown to improve cell attachment and proliferation of fibroblasts and adipose-derived stem cells (115). Both fibrillin and keratin may help stimulate a wound-healing response in the injured lung by inducing the formation of new ECM by increasing cell attachment and deposition of ECM scaffolding proteins. Another glycoprotein thrombospondin can interact with ECM structural components, growth factors, cytokines, and matricellular proteins. This includes interactions with matrix-metalloproteinase (MMP) 2 and MMP9 that can regulate collagen homeostasis and prevent the overproduction of collagen that can form fibrotic tissue (116).

Meanwhile, elastin was found only in the PL ECM nanoparticles, which corresponds to the fact that elastin is a critical component of lung ECM that allows stretch during the inhalation of air (68).

Additionally, the glycoproteins fibulin-1 and fibilin-2 were found in the MMSC ECM nanoparticles and fibulin-5 was located in the PL ECM nanoparticles. Fibulins are hypothesized to organize ECM structural fibers, including the basement membrane and elastin fibers. Fibulin 1 has been found to organize ECM fibers composed of elastin and fibrillin 1 and 2 during murine lung development. Fibulin-2 can bind to elastin and fibrillin 1, serving to attach microfibrils to elastin (117). Fibulin-5 mediates the crosslinking of tropoelastin monomers into insoluble elastin polymer and is typically found in higher levels in the lungs (114). The presence of fibulin found in the ECM nanoparticles may help repair injured ECM in the wounded lung.

According to PeptideRanker, the ECM nanoparticles contained peptides that are considered to be bioactive. Both PL and MMSC ECM contained collagen fragments, fibronectin, and laminin subunits that ranked highly on the bioactivity scale. These ECM proteins are known to release bioactive peptides upon partial proteolysis. In particular, it is known that sequences with high hydrophobicity or cationic sequences have an antimicrobial effect through interactions with the bacterial cell membrane (88).

Thrombospondins, found in the MMSC ECM nanoparticles is another ECM protein that contains a higher concentration of hydrophobic amino acids that can cause an antimicrobial effect. Tetraspanin proteins contain two extracellular loops and four hydrophobic transmembrane regions, which may destabilize the bacterial cell membrane (118,119).

In the PL ECM nanoparticles, peptides of the same family as known antimicrobial peptides were found. Protegrin 4 is a member of the protegrin family, which is from a precursor

antimicrobial peptide called cathelicidins (120). In fact, it is known that the protegrin class are active against *E. coli*, *S. aureus*, and *P. aeruginosa*, which makes it a desirable peptide to treat VAP infections. Azurocidin has been found to act effectively against gram-negative bacteria and also gram-positive bacteria (121). The mechanism behind its antimicrobial activity is unknown, but azurocidin is a member of the serprocidin family, serine proteases with antimicrobial activity (122). In addition, an acyl-CoA binding protein, which shares similarities with a bioactive peptide, was detected in the nanoparticles (123). The presence of these bioactive peptides makes the ECM nanoparticles promising antimicrobial agents on top of being able to stimulate wound healing in the lungs.

Aim 3

Methods and Materials

MTT assay: Cytotoxicity and Proliferation of MMSC ECM Nanoparticles

The MTT assay was conducted to evaluate the cytotoxicity of the MMSC ECM nanoparticles. In vitro cytotoxicity testing was critical to determine if the nanoparticles were toxic to cells before using them as a treatment in an in vivo model. The cytotoxic activity of the nanoparticles was evaluated on MMSCs and MLE-12 cells. MMSCs were tested to ensure that the nanoparticles would not affect the population of stem cells in the lungs, as stem cells help contribute to tissue repair and can differentiate into epithelial cells (124). MLE-12 cells were used in the assay to ensure the nanoparticles would not induce necrosis in the lung epithelial layer.

To evaluate the cytotoxic effects of the nanoparticles, cells were seeded at a density of 10,000 per well and grown in a 96-well plate (Falcon) for 48 hours. Media was then replaced with nanoparticle treatments with concentrations of 0.50 ng/mL, 1.0 ng/mL, 2.0 ng/mL, and 4.0 ng/mL, or replenished with new media. An 2.8% ethanol control solution was tested as well to ensure a slight percentage of ethanol in the nanoparticle solution (concentration of ethanol was from 4.0 ng/mL concentration was unharmful to the cells). Treatments were added for 24 hours then the procedure from the MTT assay was conducted (Roche).

To determine if ECM nanoparticles increased cellular proliferation, ECM nanoparticle treatment, in concentrations of 0.50 ng/mL, 1.0 ng/mL, 2.0 ng/mL, and 4.0 ng/mL were added to 10,000 cells in a 96-well plate (Falcon) at the same time. This was repeated with cell culture media, conditioned media with secreted ECM proteins, and 2.8% ethanol solution as controls. The cells were grown for 24 hours then MTT assay (Roche) procedure was followed.

Scratch Assay

Human lung fibroblast cells were used for the scratch assay to evaluate whether the ECM nanoparticles stimulate wound healing. Fibroblasts are critical in the healing process, as they secrete growth factors, cytokines, and ECM to repair an injury (125). 200,000 cells were seeded into a 6-well cell culture plate, marked with a horizontal line on the bottom using a sterile straight edge. Cells were incubated at 37°C to grow overnight.

The next day a 20 µl pipette tip was used to scratch the cell layer perpendicular to the horizontal like at the bottom of the well. The media was aspirated from each well and then washed with 1 mL HEPES. Media supplemented with nanoparticles in concentrations of 0.50 ng/mL, 1.0 ng/mL, 2.0 ng/mL, and 4.0 ng/mL, was then applied. Media without any nanoparticles was used as a control. Once the media was applied, the wells were imaged using a phase contrast microscope to determine the initial area of the scratch. Pictures were taken above and below the horizontal line applied on the well. The well plate was incubated for 48 hours after the scratch to determine the closure rate, pictures were taken every 24 hours. Once images were collected, ImageJ software was used to determine the area of the scratch and the closure rate for each treatment was calculated (126). The following formula was used to calculate the area of the scratch:

$$\text{Percentage of Wound Healed} = [\text{Area}(T_0) - \text{Area}(T_X)] / \text{Area}(T_0).$$

Area(T_0) was the initial denuded area for each image location. Area(T_X) was the denuded area for each location after 24 or 48 hours.

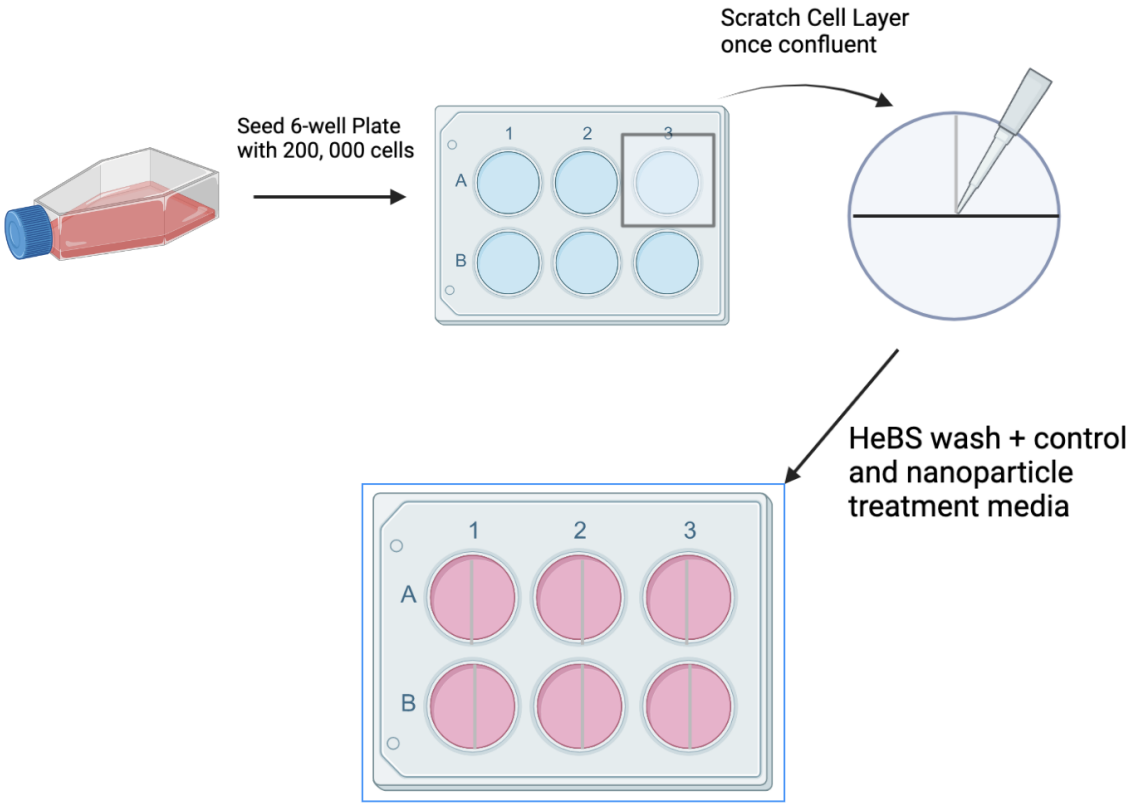

Figure 15. Procedure for Scratch Assay.

Statistical Analysis

All statistical analyses were performed using Prism 9 (GraphPad). Ordinary analyses of variance with multiple comparisons were used to determine the significance of the results. Significant results were determined to have a p-value < 0.05.

Results

MTT assay: Cytotoxicity and Proliferation of MMSC ECM Nanoparticles

MMSC ECM nanoparticles were determined to be biocompatible with mouse lung epithelial cells and increase cellular proliferation. The ethanol control was found to not induce cell necrosis, indicating the slight amount of ethanol in the nanoparticle media was not responsible for the effects of the experiment. Nanoparticles were cultured with MLE-12 cells for 24 hours then the MTT assay was performed. Both nanoparticle concentrations of 0.5 ng/mL and 1.0 ng/mL significantly increased the cellular proliferation, as they were both approximately 80% more confluent than the media-only well. When added to a confluent layer of MLE-12 cells, the concentrations of 0.50 ng/mL, 1.0 ng/mL, 2.0 ng/mL, and 4.0 ng/mL only decreased cellular proliferation by 15.4% at most after 48 hours.

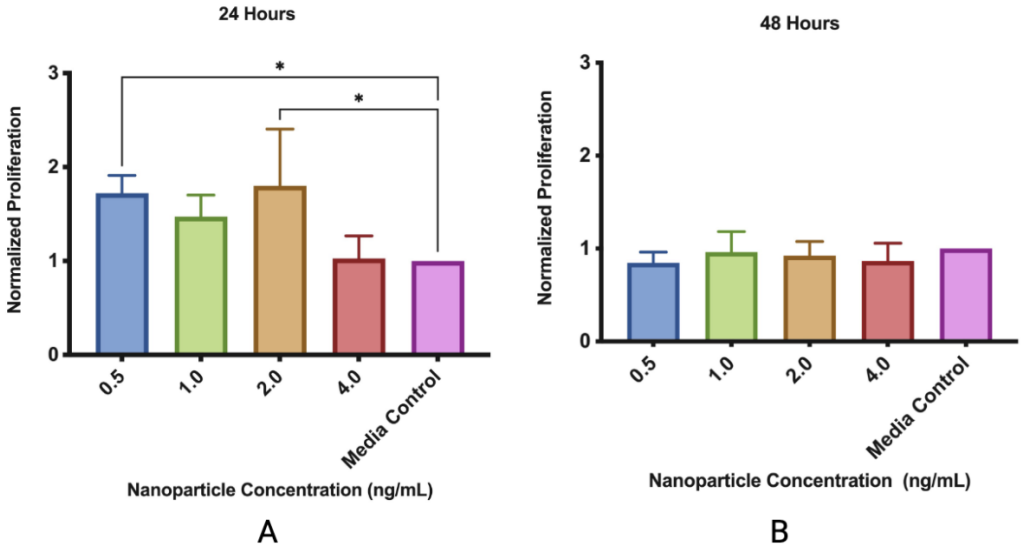

Figure 16. MMSC ECM Nanoparticles are biocompatible and can increase cellular proliferation. A) MMSC ECM Nanoparticles were added with MLE-12 Cells for 24 hours to test proliferative

effects B)MMSC ECM Nanoparticles were added to MLE-12 Cells for 48 hours to test cytotoxicity. Data displayed is the mean± standard deviation. * indicates $p < 0.05$. N=3

MMSC ECM nanoparticles were then applied to MMSCs and determined to be non-cytotoxic and slightly increase cellular proliferation. After 24 hours, MMSC viability was shown to improve when supplemented with 2.0 ng/mL and 4.0 ng/mL of MMSC ECM nanoparticles, increasing cell count by 5% and 3% respectively. This effect continued to occur as the nanoparticles increased cellular proliferation when applied to a confluent cell layer of MMSCs for 48 hours. The nanoparticle concentration of 2.0 ng/mL had the greatest effect as it increased proliferation by 7% compared to the media alone. Even though cellular proliferation was not significantly improved when supplemented with nanoparticle media, the results indicate that the nanoparticles are not cytotoxic to MMSCs.

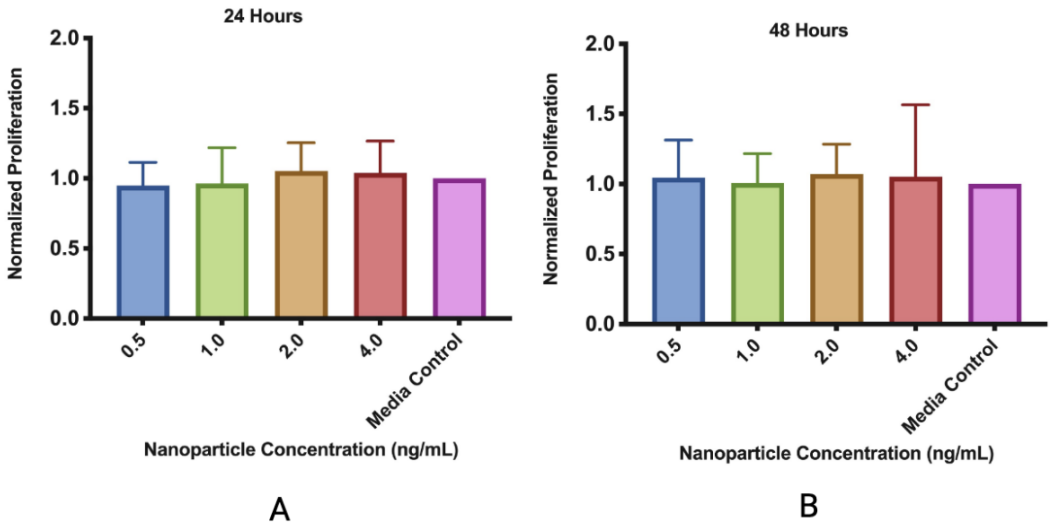

Figure 17. MMSC ECM Nanoparticles are biocompatible and can increase cellular proliferation. A) MMSC ECM Nanoparticles were added with MMSCs for 24 hours to test proliferative

effects. B)MMSC ECM Nanoparticles were added to MMSCs for 48 hours to test cytotoxicity. Data displayed is the mean± standard deviation. N=3.

Scratch Assay

After the fibroblast cell layer was scratched, nanoparticles in concentrations of 0.5 ng/mL, 1.0 ng/mL, 2.0 ng/mL, and 4.0 ng/mL were applied in supplemented media. Closure rates based on ImageJ were calculated. After 24 hours, media with nanoparticles in a concentration of 4.0 ng/mL had the greatest effect on the healing of the scratch, as it increased the closure rate of the scratch by 80% compared to the media control. The concentrations of 0.5 ng/mL, 1.0 ng/mL, and 2.0 ng/mL all increased the rate of closure significantly as well as compared to the media alone. As the concentration of nanoparticles increased in the media, the rate of scratch closure increased as well. After 48 hours, the scratches from the nanoparticle treatment groups were closed while the scratch supplemented with the media control was on average 87% healed.

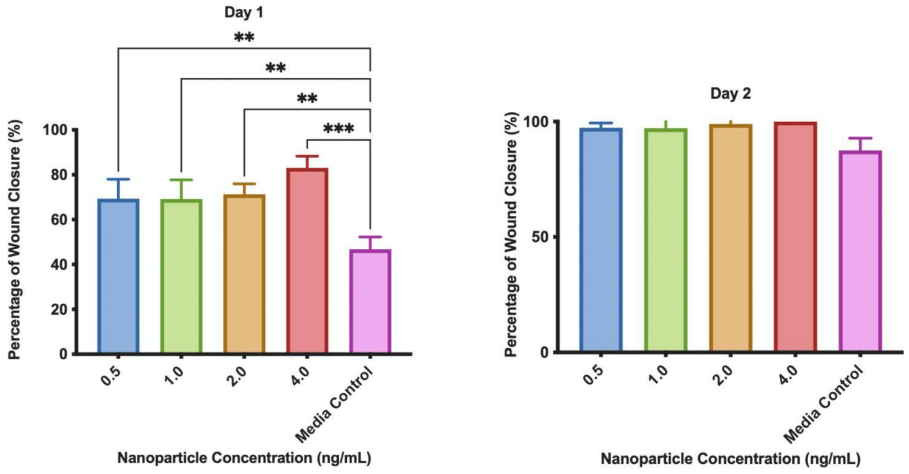

A B

Figure 18. Scratch Assay Results. Fibroblasts supplemented with MMSC ECM Nanoparticles have a higher growth rate compared to the media control. A) Fibroblast Growth Rate after 24 hours with Nanoparticle Media. B) Fibroblast Growth Rate after 48 hours with Nanoparticle Media. Data displayed is the mean± standard deviation. * indicates $p< 0.05$, ** indicates $p<0.001$, *** indicates $p<0.0001$, N=3.

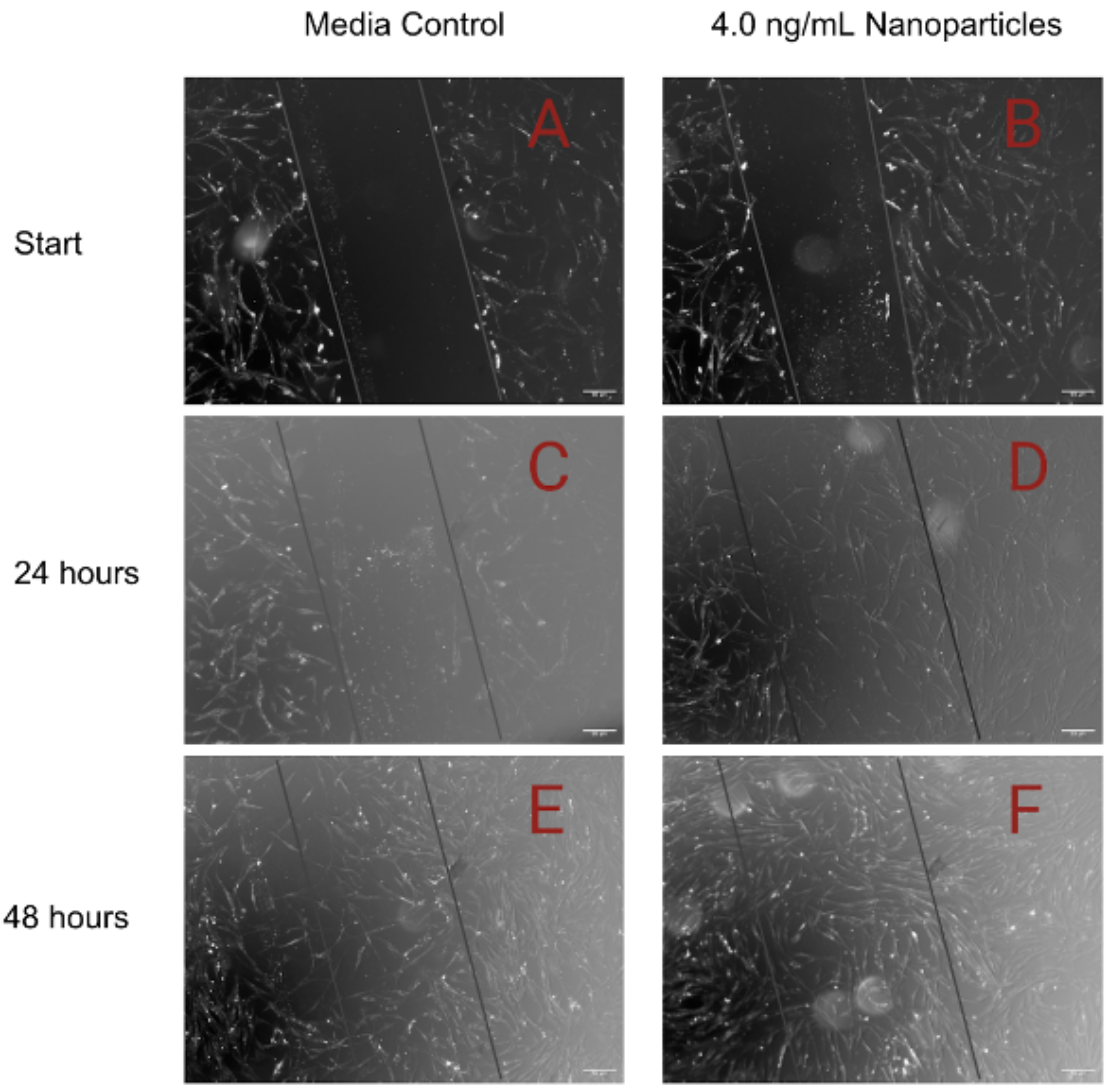

Figure 19. Scratch Assay Images of Human Lungs Fibroblasts. Confluent cell sheets were scratched and replenished with media (left) or 4.0 ng/mL of MMSC ECM Nanoparticles (right).

Images were obtained every 24 hours. The scratch was closed at a faster rate with the supplementation of nanoparticles. A: Media, 0 hours B: 4.0 ng/mL Nanoparticles, 0 hours C: Media, 24 hours D: 4.0 ng/mL Nanoparticles, 24 hours E: Media, 48 hours F: 4.0 ng/mL Nanoparticles, 48 hours.

Discussion

The MTT assays for 24 and 48 hours show that the MMSC ECM nanoparticles are biocompatible. Once nanoparticles were applied to a pre-seeded epithelial cell layer that was grown for 48 hours, cell count was slightly increased compared to media alone, which indicated that the nanoparticles did not induce cell death. From these promising results, it suggests that when interacting with the lung epithelium, the ECM nanoparticles will not induce further damage on injuring wounded tissue.

Similarly, the MMSC ECM nanoparticles were biocompatible with MMSCs. This may be due to the ability of MSC secretome, in the form of dECM, to encourage the growth of MSCs as we are adding their own cellular product into the media to support growth (127). Our ECM nanoparticles may be about to support MSCs in the lung. When applied to an injured lung, the nanoparticles may help activate the lung MSCs which can them work to issue a wound-healing response and regenerate lung tissue.

We showed that our nanoparticles encourage wound closure and cellular attachment when applied to lung fibroblasts. All concentrations of our MMSC ECM nanoparticles closed the scratch at a significantly faster rate than the media alone. An increased wound closure rate may be critical for a patient's condition. Cells can begin to deposit on injured tissue quickly to start to re-epithelization process, restoring barrier function and proper gas exchange in the lungs.

Fibroblasts are the main cellular source of the ECM, so the repair of lung fibroblasts is critical to supporting new cell and tissue development (128). Fibroblasts serve another important role in the lung, modulating differentiation, and proliferation of alveolar epithelial cells (129). Their vitality is then critical to repairing damaged lung epithelium. MSCs have been reported to recruit fibroblasts to an injury site and our MMSC ECM nanoparticles show a similar effect by increasing the rate of wound closure (96). The ECM protein fragments found in the nanoparticles may help stimulate the production of a new layer of ECM, which may explain the rapid wound closure.

The MMSC ECM nanoparticles are able to promote cell viability of epithelial, MSC, and fibroblast cells, all important components of the lung environment. With these promising results *in vitro*, it may be possible to see the effects of the ECM nanoparticles in an *in vivo* model.

Aim 4

Methods and Materials

Inhibition of Bacterial Growth

An overnight culture was prepared by taking a colony of wild-type *Escherichia coli* HfrH from a streak plate and submerging it in 5 ml of LB broth. The culture was incubated in a shaking incubator at 37℃ and 200 rpm. The following day 100 µl of that overnight culture was added to 10 ml of LB broth. MMSC ECM nanoparticles were added in concentrations of 4.0 ng/mL and 0.50 ng/mL and PL ECM nanoparticles of 6.4 ng/mL and 0.80 ng/mL were added to the culture. An LB broth control without nanoparticles was used as a control. Flasks were shaken overnight at 200 rpm at 37℃. At the time points of 1 hour, 3 hours, 6 hours, and 24 hours, 100 µl of the culture was taken and spread onto an agar plate, which was left to incubate overnight. The next day colonies grown on the plate were counted and analyzed. The procedure was utilized for testing if the nanoparticles inhibit the growth of *Staphylococcus aureus* Newman and *Pseudomonas aeruginosa* PAO1.

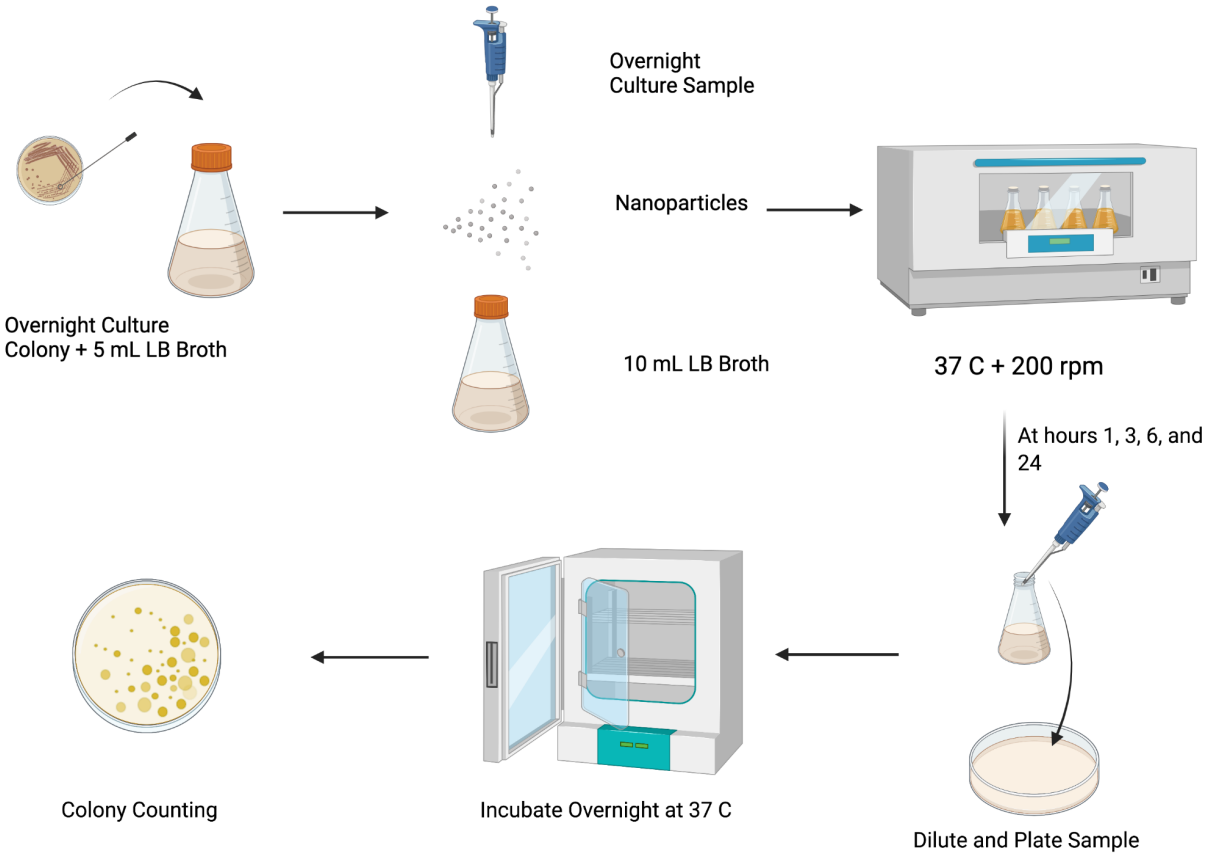

Figure 20. Bacterial Assay Procedure.

Statistical Analysis

All statistical analyses were performed using Prism 9 (GraphPad). Ordinary analyses of variance with multiple comparisons were used to determine the significance of the results. Significant results were determined to have a p-value < 0.05.

Results

Inhibition of Bacterial Growth

Both MMSC and PL ECM nanoparticles are able to inhibit the growth of bacterial wild-type strains. While PL ECM nanoparticles did not display growth inhibition of gram-negative *E.coli,* MMSC ECM nanoparticles inhibited growth at a concentration of 4.0 ng/mL. Nanoparticles began to impede growth around hour 3 and significantly reduced bacterial growth after 6 and 24 hours of culture incubation.

PL ECM nanoparticles had a positive effect on slowing the growth of gram-positive *S. aureus*, while the MMSC ECM nanoparticles did not show any ability to inhibit the growth of *S. aureus*. A lower concentration of PL ECM nanoparticles inhibited bacterial growth the best out of all tested nanoparticle concentrations. *S. aureus* growth was reduced for 24 hours and at 3 hours growth was significantly lower than the LB broth control.

Against *P. aeruginosa*, both MMSC and PL ECM nanoparticles display antibacterial effects. Both MMSC and PL ECM nanoparticles lowered bacterial growth over 24 hours, and growth was significantly reduced at 3 hours for MMSC ECM nanoparticles and 6 hours for PL ECM nanoparticles.

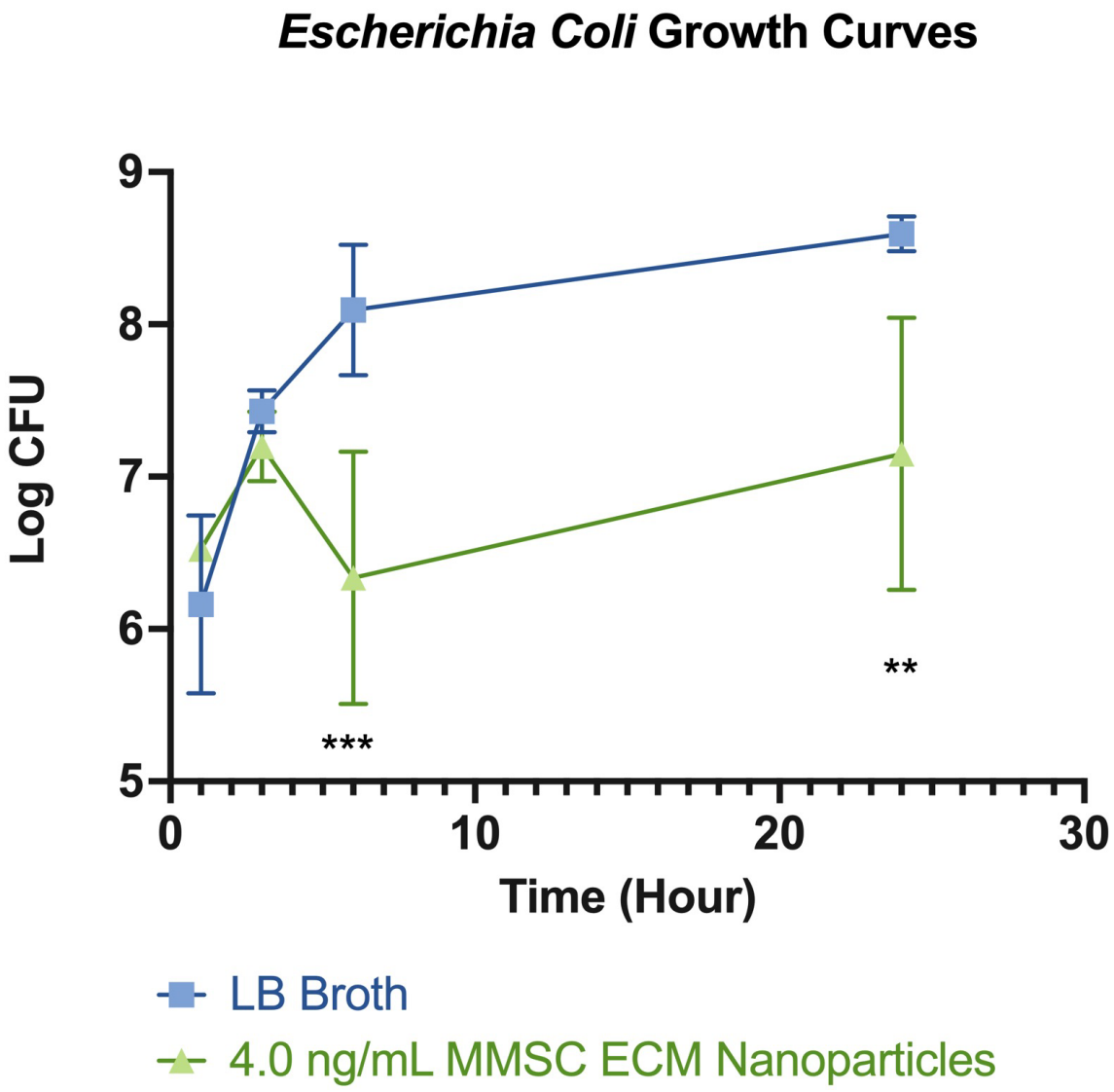

Figure 21. Comparison of *E. coli* growth curves for LB Broth control culture and 4.0 ng/mL MMSC ECM Nanoparticle culture. MMSC ECM Nanoparticles show inhibition of *E. coli* growth at hours 3, 6, and 24. Growth inhibition was significant at 6 hours and 24 hours of incubation. Data displayed is the mean± standard deviation. * indicates $p< 0.05$, ** indicates $p<0.001$, *** indicates $p<0.0001$. N=3.

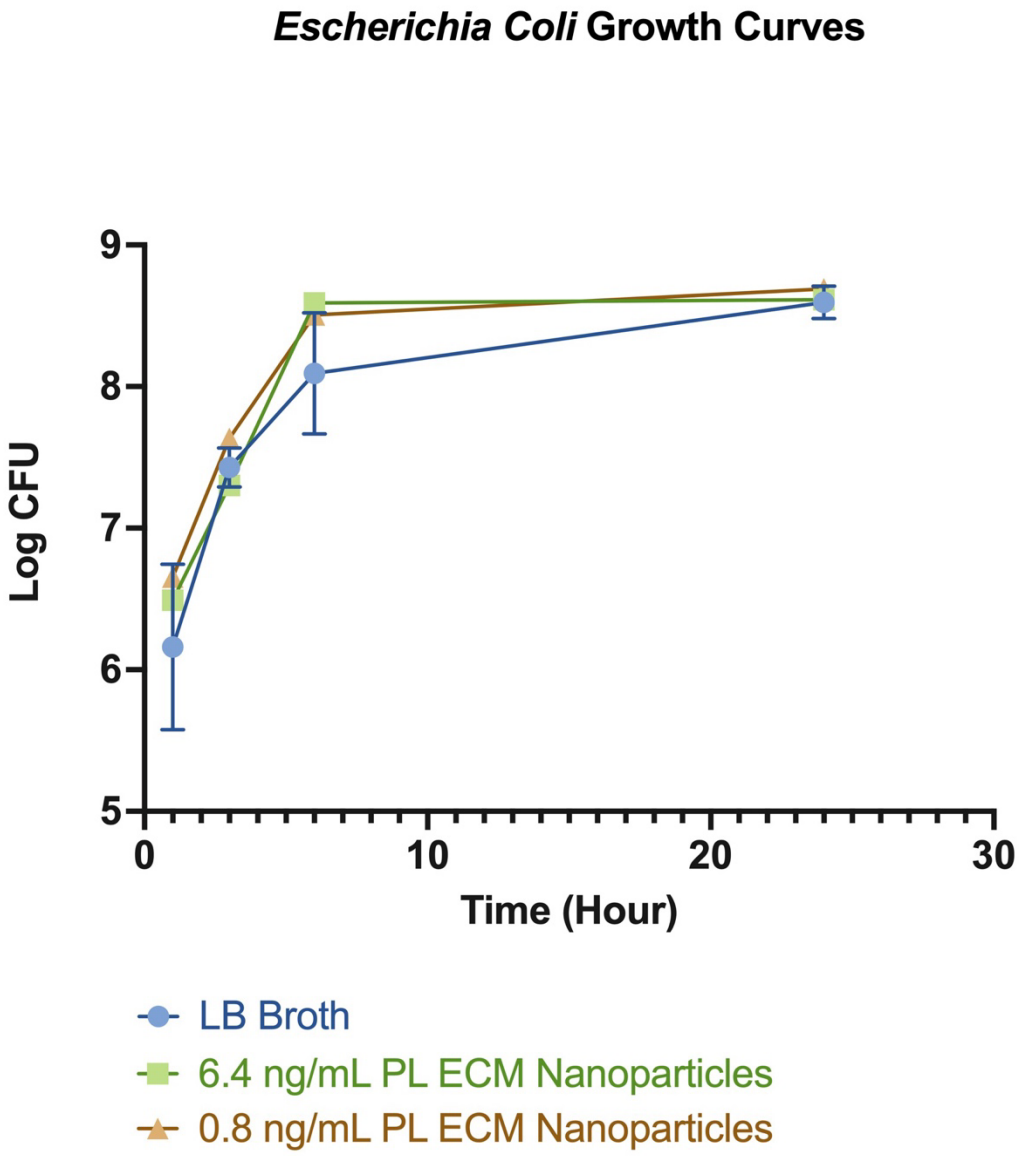

Figure 22. Comparison of *E. coli* growth curves for LB Broth control culture, 6.4 ng/mL PL ECM Nanoparticle culture, and 0.8 ng/mL PL ECM Nanoparticle culture. PL ECM Nanoparticles did not show any growth inhibition of *E. coli*. Data displayed is the mean± standard deviation. * indicates $p< 0.05$, ** indicates $p<0.001$, *** indicates $p<0.0001$. L. Broth N=3, 6.4 ng/mL PL ECM Nanoparticle culture and 0.8 ng/mL PL ECM Nanoparticle culture N=1.

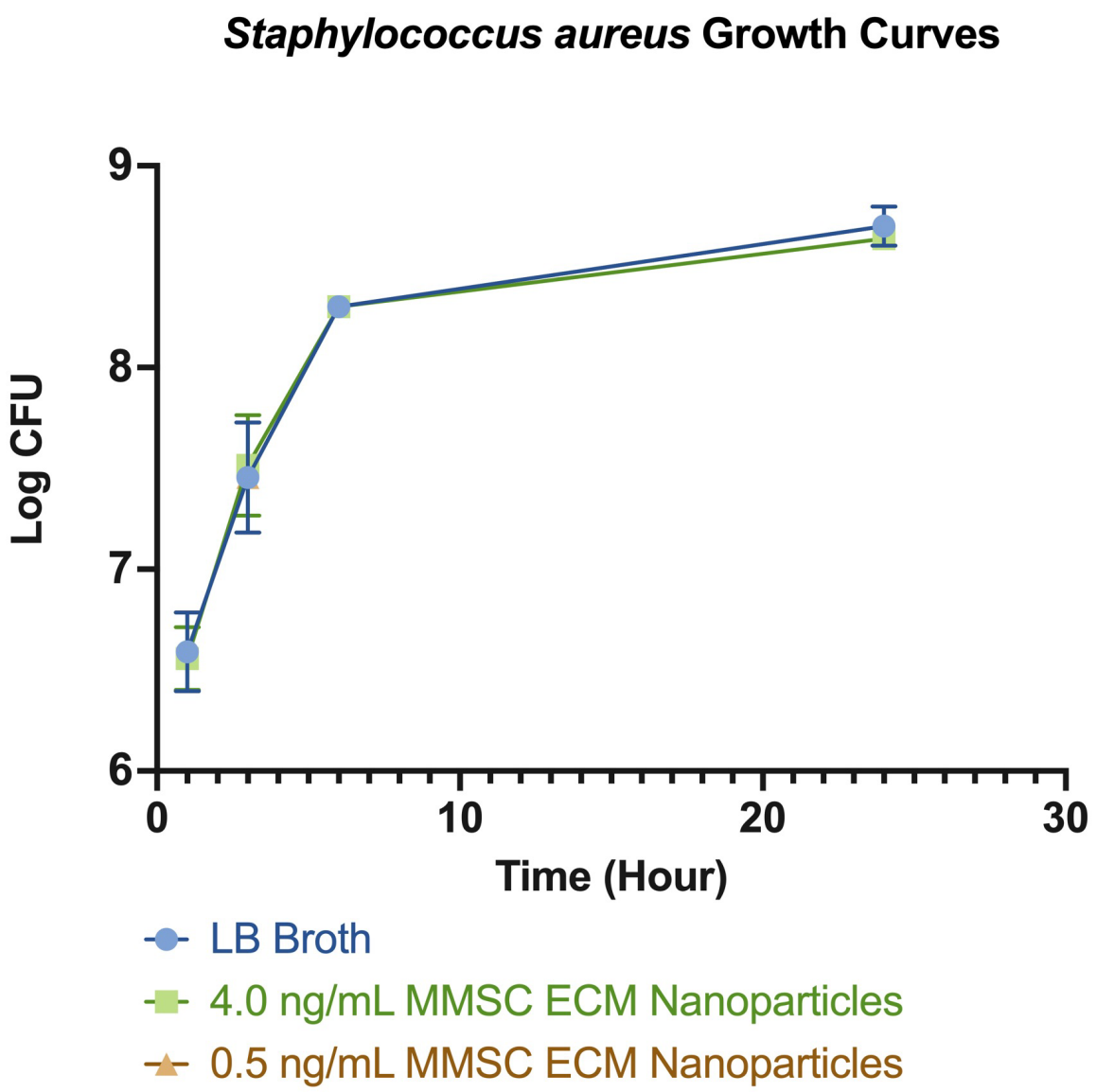

Figure 23. Comparison of *S. aureus* growth curves for LB Broth control culture, 4.0 ng/mL MMSC ECM Nanoparticle culture, and 0.5 ng/mL MMSC ECM Nanoparticle culture. MMSC ECM Nanoparticles do not show inhibition of *S. aureus* growth at hours 3, 6, and 24. Data displayed is the mean± standard deviation. * indicates $p< 0.05$, ** indicates $p<0.001$, *** indicates $p<0.0001$. N=3.

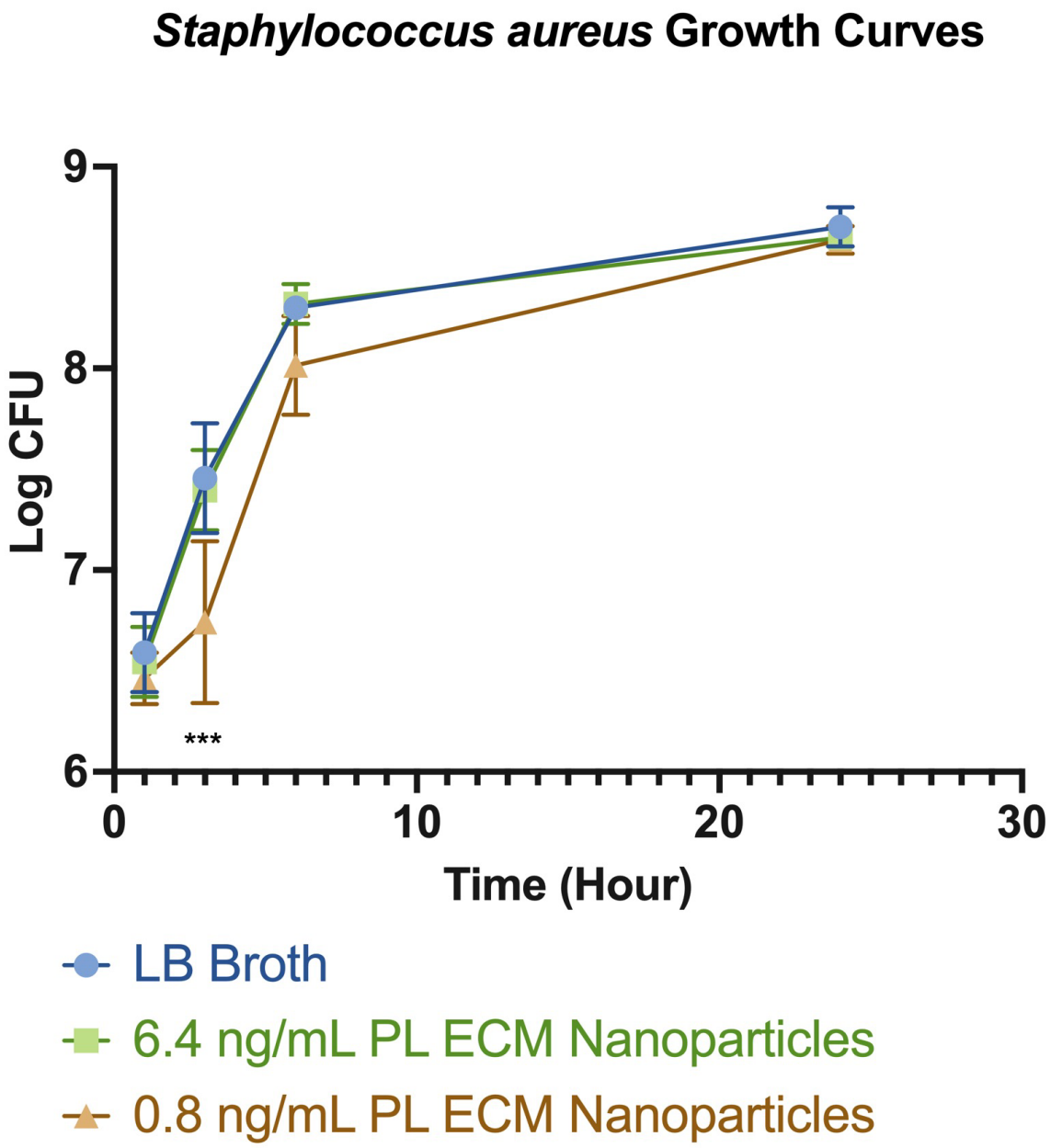

Figure 24. Comparison of *S. aureus* growth curves for LB Broth control culture, 6.4 ng/mL PL ECM nanoparticle culture, and 0.8 ng/mL PL ECM nanoparticle culture. PL ECM nanoparticles show inhibition of *S. aureus* growth at hours 1, 3, and 6. Data displayed is the mean± standard deviation. * indicates $p< 0.05$, ** indicates $p<0.001$, *** indicates $p<0.0001$. The concentration of 0.8 ng/mL PL ECM nanoparticles was found to be significantly different after 3 hours of incubation. N=3.

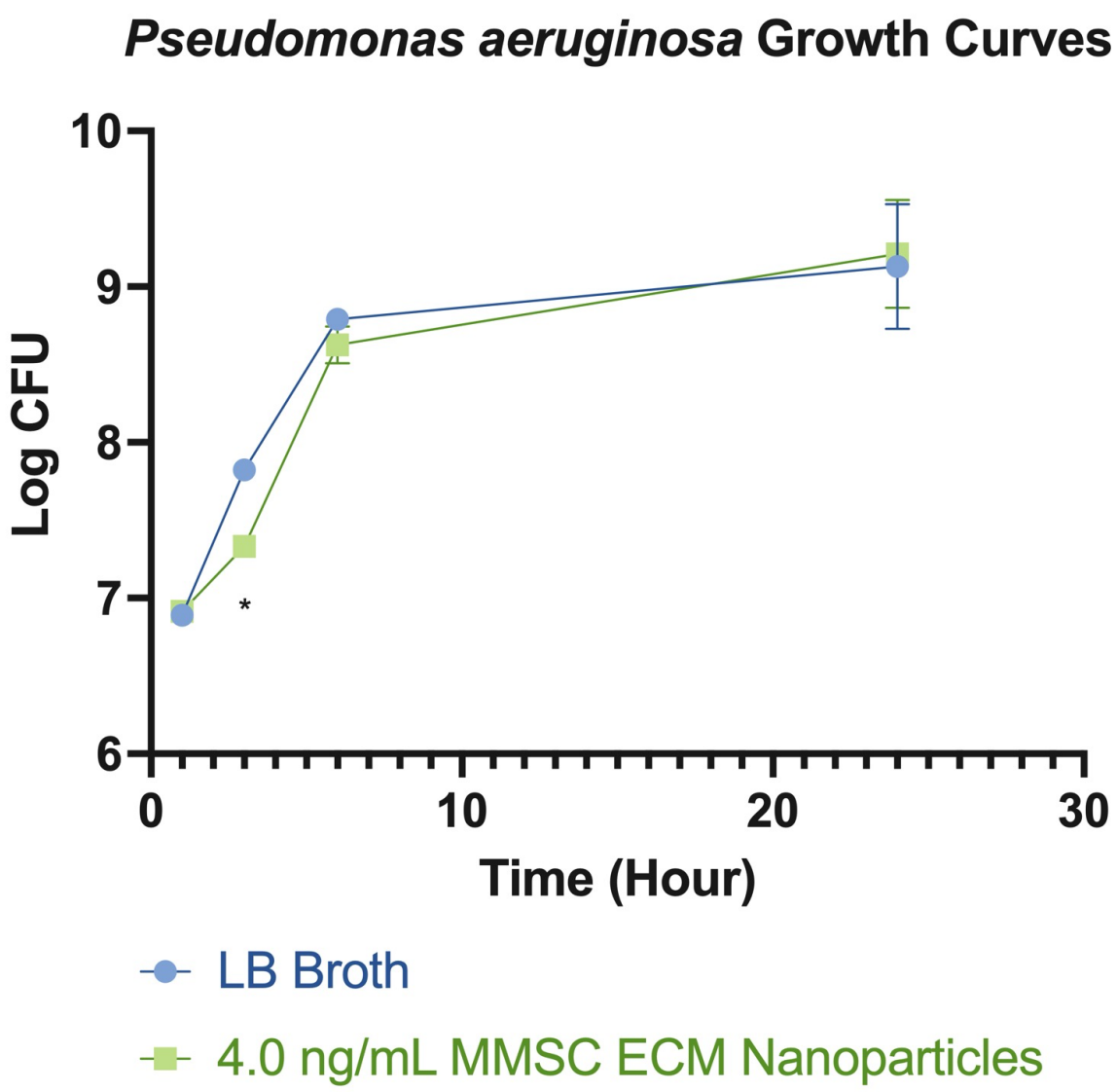

Figure 25. Comparison of *P. aeruginosa* growth curves for LB Broth control culture and 4.0 ng/mL MMSC ECM Nanoparticle culture. MMSC ECM Nanoparticles show inhibition of *P. aeruginosa* growth at hour 3. Data displayed is the mean± standard deviation. * indicates $p< 0.05$, ** indicates $p<0.001$, *** indicates $p<0.0001$. The concentration of 4.0 ng/mL MMSC ECM nanoparticles was found to be significantly different after 3 hours of incubation. N=3.

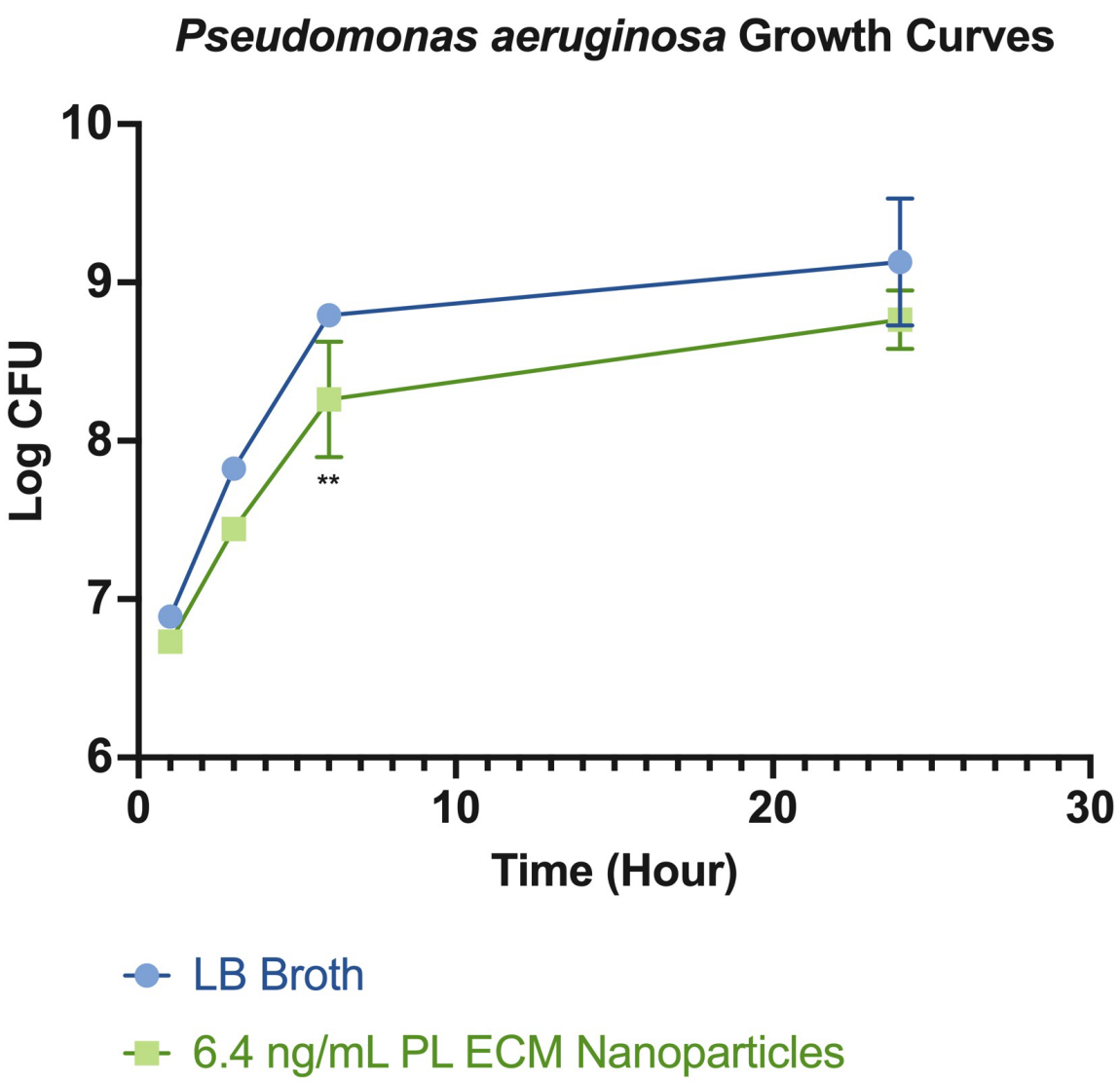

Figure 26. Comparison of *P. aeruginosa* growth curves for LB Broth control culture and 6.4 ng/mL PL ECM Nanoparticle culture. PL ECM Nanoparticles show inhibition of *P. aeruginosa* growth at hours 1,3,6, and 24. Data displayed is the mean± standard deviation. * indicates $p< 0.05$, ** indicates $p<0.001$, *** indicates $p<0.000$. The concentration of 6.4 ng/mL PL ECM nanoparticles display significantly less growth at 6 hours. N=3.

Discussion

It was shown that the ECM nanoparticles have antimicrobial properties. The MMSC ECM nanoparticles were effective at inhibiting the growth of *E. coli* and *P. aeruginosa*, while the PL ECM nanoparticles effectively reduced the growth of *S. aureus* and *P. aeruginosa*. Most antimicrobial effects were displayed at hours 1-6, which matches the timeframe the nanoparticles would remain in the lungs before clearance. The mass spectrometry analysis revealed some antimicrobial peptides that may be responsible for these effects. The MMSC ECM nanoparticles contain thrombospondin which is characterized by hydrophobic regions that will interact with the bacterial membrane in both gram-positive and gram-negative bacteria. The nanoparticles also contained the beta-1 chain of laminin, which is composed of highly cationic peptide sequences that can interact with the negative surface charge of the bacteria and induce an antimicrobial effect. The PL ECM nanoparticles were composed of collagen type VI which also reportedly has several of these cationic regions (88). Both ECM nanoparticles contain other forms of collagen, laminin, and glycoproteins that may contribute to the antimicrobial ability of the ECM nanoparticles.

Although it is not fully understood, there are a few mechanisms that propose how antimicrobial peptides inhibit the growth of bacteria. As peptides contain hydrophobic and cationic regions, they can interact with the lipopolysaccharides of the gram-negative membrane or teichoic acid and peptidoglycans in the gram-positive membrane (88). These interactions can induce conformational changes in the cell wall, causing bacteria cell necrosis (130). Positive peptide sequences can disrupt the lipid sequence of bacterial membranes by clustering lipids in one region due to the attraction to the cationic peptides, which stops cell growth (131). The binding of the cationic peptide to a negatively charged lipid can also destabilize the charge of the bacterial cell membrane (132). Through electrostatic interactions, the peptide can insert itself

into the lipid bilayer and form a pore in the structure of the membrane (88). Instead of permeabilizing the membrane, AMPs can also bind to intracellular targets to stop metabolic processes. AMPs, such as Buforin II, are found to directly bind to DNA and RNA molecules after entering the bacterial cell (133).

Conclusion

We have developed and characterized nanoparticles made from the ECM of MMSCs. The decellularization method that was utilized to isolate the ECM from the MMSCs was shown to retain the ECM proteins collagen and GAG while reducing cellular DNA of MMSCs. The nanoparticles were fabricated with a negative charge and 50-300 nm size to reach the distal regions of the lungs. After the introduction of the nanoparticles to both MLE-12 and MMSC cells, the nanoparticles did not significantly decrease cellular viability and displayed properties of being biocompatible. The MMSC ECM nanoparticles were shown to be composed of peptides that promote wound healing of injured tissues while inhibiting the growth of bacteria. This combination of properties makes them an ideal treatment for ARDS as the nanoparticles are capable of reaching the distal regions of the lungs while preventing bacterial infection if the patient needs mechanical ventilation treatment.

Future Directions

For future evaluation of the nanoparticles, we can further examine the mass spectrum to discover which exact antimicrobial peptides are responsible for the wound healing and antimicrobial effects of the nanoparticles. Specific peptides with pro-regenerative or antimicrobial effects may also be loaded into the nanoparticles to increase the efficacy of the treatment or improve scaffolding for new cellular growth.

To optimize the nanoparticle treatment, dosage studies will occur to find the ideal concentration of nanoparticles that remains biocompatible, and also promotes wound healing and inhibits the growth of bacteria. The concentrations that were tested in this study were minimal, so increasing the concentration of our nanoparticles may improve upon their bioactive effects. Future studies can also examine using multiple doses of nanoparticle treatment over the course of several days, as bacterial growth was only inhibited in the 1–6-hour range.

Moreover, an antibiotic can be loaded into the nanoparticles to increase the efficacy of the treatment against bacteria. The antibiotic can be digested along with the decellularized ECM and then formed into a nanoparticle using electrospray deposition. A broad-spectrum antibiotic, such as levofloxacin, can be added to improve the effects of the antimicrobial peptides found in our ECM nanoparticles against both gram-positive and gram-negative bacteria.

Additionally, nanoparticles can be converted into an aerosolized treatment that can be administered through inhalation. Aerosolized treatments continue to be the most popular form of lung treatment delivery, as it allows for direct and rapid delivery to injured lung tissue. An aerosolized form of the nanoparticles can be delivering during a mechanical ventilation regiment, which may help reduce ventilator damage to the lungs, improve lung function, and prevent bacterial infection.

Appendix I

For further information, portions of this thesis are also presented in Wandling et al:

Wandling, E.N.; Rhoads, K.; Ohman, D.E.; Heise, R.L. Electrosprayed Mesenchymal Stromal Cell Extracellular Matrix Nanoparticles Accelerate Cellular Wound Healing and Reduce Gram-Negative Bacterial Growth. *Pharmaceutics* 2023, *15*, 1277. https://doi.org/10.3390/pharmaceutics15041277

References

1. Walkey, A. J., Summer, R., Ho, V., & Alkana, P. (2012). Acute respiratory distress syndrome: epidemiology and management approaches. *Clinical Epidemiology*, *4*(1), 159. https://doi.org/10.2147/CLEP.S28800
2. Matthay, M. A., Zemans, R. L., Zimmerman, G. A., Arabi, Y. M., Beitler, J. R., Mercat, A., Herridge, M., Randolph, A. G., & Calfee, C. S. (2019). Acute respiratory distress syndrome. *Nature Reviews. Disease Primers*, *5*(1).
3. Alhazzani, W., Møller, M. H., Arabi, Y. M., Loeb, M., Gong, M. N., Fan, E., Oczkowski, S., Levy, M. M., Derde, L., Dzierba, A., Du, B., Aboodi, M., Wunsch, H., Cecconi, M., Koh, Y., Chertow, D. S., Maitland, K., Alshamsi, F., Belley-Cote, E., … Rhodes, A. (2020). Acute Respiratory Distress Syndrome: Diagnosis and Management. *American Family Physician*, *101*(12), 730–738. https://doi.org/10.1007/S00134-020-06022-5
4. Radbel, J., Laskin, D. L., Laskin, J. D., & Kipen, H. M. (2020). Disease-modifying treatment of chemical threat agent–induced acute lung injury. *Annals of the New York Academy of Sciences*, *1480*(1), 14–29. https://doi.org/10.1111/NYAS.14438
5. Parcha, V., Kalra, R., Bhatt, S. P., Berra, L., Arora, G., & Arora, P. (2021). Trends and Geographic Variation in Acute Respiratory Failure and ARDS Mortality in the United States. *Chest*, *159*(4), 1460. https://doi.org/10.1016/J.CHEST.2020.10.042
6. Diamond, M., Feliciano, H. L. P., Sanghavi, D., & Mahapatra, S. (2022). Acute Respiratory Distress Syndrome. *StatsPearls[Internet]*. https://www.ncbi.nlm.nih.gov/books/NBK436002/
7. Boyle, A. J., Sweeney, R. M., & McAuley, D. F. (2013). Pharmacological treatments in ARDS; a state-of-the-art update. *BMC Medicine*, *11*(1), 1–7. https://doi.org/10.1186/1741-7015-11-166/TABLES/2

8. *Acute Respiratory Distress Syndrome - Treatment | NHLBI, NIH*. (2022, March 24). National Heart, Lung, and Blood Institute. https://www.nhlbi.nih.gov/health/ards/treatment
9. Fan, E., Brodie, D., & Slutsky, A. S. (2018). Acute Respiratory Distress Syndrome: Advances in Diagnosis and Treatment. *JAMA*, *319*(7), 698–710. https://doi.org/10.1001/JAMA.2017.21907
10. Koenig, S. M., & Truwit, J. D. (2006). Ventilator-Associated Pneumonia: Diagnosis, Treatment, and Prevention. *Clinical Microbiology Reviews*, *19*(4), 637. https://doi.org/10.1128/CMR.00051-05
11. Han, S., & Mallampalli, R. K. (2015a). The acute respiratory distress syndrome: from mechanism to translation. *Journal of Immunology (Baltimore, Md. : 1950)*, *194*(3), 855. https://doi.org/10.4049/JIMMUNOL.1402513
12. Swenson, K. E., & Swenson, E. R. (2021). Pathophysiology of Acute Respiratory Distress Syndrome and COVID-19 Lung Injury. *Critical Care Clinics*, *37*(4), 749. https://doi.org/10.1016/J.CCC.2021.05.003
13. Wang, Y., Tang, Z., Huang, H., Li, J., Wang, Z., Yu, Y., Zhang, C., Li, J., Dai, H., Wang, F., Cai, T., & Tang, N. (2018). Pulmonary alveolar type I cell population consists of two distinct subtypes that differ in cell fate. *Proceedings of the National Academy of Sciences of the United States of America*, *115*(10), 2407–2412. https://doi.org/10.1073/PNAS.1719474115/SUPPL_FILE/PNAS.1719474115.SD07.XLSX

14. Han, S. H., & Mallampalli, R. K. (2015). The role of surfactant in lung disease and host defense against pulmonary infections. *Annals of the American Thoracic Society*, *12*(5), 765–774.
15. Cardinal-Fernandez, P., Lorente, J. A., Ballen-Barragan, A., & Matute-Bello, G. (2017). Acute respiratory distress syndrome and diffuse alveolar damage new insights on a complex relationship. *Annals of the American Thoracic Society*, *14*(6), 844–850. https://doi.org/10.1513/ANNALSATS.201609-728PS/SUPPL_FILE/DISCLOSURES.PDF
16. Kosyreva, A., Dzhalilova, D., Lokhonina, A., Vishnyakova, P., & Fatkhudinov, T. (2021). The Role of Macrophages in the Pathogenesis of SARS-CoV-2-Associated Acute Respiratory Distress Syndrome. *Frontiers in Immunology*, *12*, 1667. https://doi.org/10.3389/FIMMU.2021.682871/BIBTEX
17. Matthay, M. A., & Zemans, R. L. (2011a). The Acute Respiratory Distress Syndrome: Pathogenesis and Treatment. *Annual Review of Pathology*, *6*, 147.
18. Glass, D. S., Grossfeld, D., Renna, H. A., Agarwala, P., Spiegler, P., DeLeon, J., & Reiss, A. B. (2022). Idiopathic pulmonary fibrosis: Current and future treatment. *The Clinical Respiratory Journal*, *16*(2), 84–96. https://doi.org/10.1111/CRJ.13466
19. Marshall, R., Bellingan, G., & Laurent, G. (1998a). The acute respiratory distress syndrome: fibrosis in the fast lane. *Thorax*, *53*(10), 815–817.
20. Adegunsoye, A., & Balachandran, J. (2015). Inflammatory Response Mechanisms Exacerbating Hypoxemia in Coexistent Pulmonary Fibrosis and Sleep Apnea. *Mediators of Inflammation*, *2015*. https://doi.org/10.1155/2015/510105

21. Tomashefski, J. F. (2000). PULMONARY PATHOLOGY OF ACUTE RESPIRATORY DISTRESS SYNDROME. *Clinics in Chest Medicine*, *21*(3), 435–466. https://doi.org/10.1016/S0272-5231(05)70158-1

22. Todd, N. W., Luzina, I. G., & Atamas, S. P. (2012). Molecular and cellular mechanisms of pulmonary fibrosis. *Fibrogenesis & Tissue Repair 2012 5:1*, *5*(1), 1–24. https://doi.org/10.1186/1755-1536-5-11

23. *Pulmonary fibrosis - Symptoms and causes - Mayo Clinic*. (n.d.). Mayo Foundation for Medical Education and Research . Retrieved January 19, 2023, from https://www.mayoclinic.org/diseases-conditions/pulmonary-fibrosis/symptoms-causes/syc-20353690

24. Hussain, M., Syed, S. K., Fatima, M., Shaukat, S., Saadullah, M., Alqahtani, A. M., Alqahtani, T., Emran, T. bin, Alamri, A. H., Barkat, M. Q., & Wu, X. (2021). Acute Respiratory Distress Syndrome and COVID-19: A Literature Review. *Journal of Inflammation Research*, *14*, 7225. https://doi.org/10.2147/JIR.S334043

25. Pfortmueller, C. A., Spinetti, T., Urman, R. D., Luedi, M. M., & Schefold, J. C. (2021). COVID-19-associated acute respiratory distress syndrome (CARDS): Current knowledge on pathophysiology and ICU treatment – A narrative review. *Best Practice & Research. Clinical Anaesthesiology*, *35*(3), 351. https://doi.org/10.1016/J.BPA.2020.12.011

26. Aslan, A., Aslan, C., Zolbanin, N. M., & Jafari, R. (2021). Acute respiratory distress syndrome in COVID-19: possible mechanisms and therapeutic management. *Pneumonia 2021 13:1*, *13*(1), 1–15. https://doi.org/10.1186/S41479-021-00092-9

27. Czajkowska-Malinowska M, Kania A, Kuca PJ, Nasiłowski J, Skoczyński S, Sokołowski R, Śliwiński PS. Treatment of acute respiratory failure in the course of COVID-19.

Practical hints from the expert panel of the Assembly of Intensive Care and Rehabilitation of the Polish Respiratory Society. Adv Respir Med. 2020;88(3):245-266. doi: 10.5603/ARM.2020.0109. PMID: 32706108.

28. Ochiai, R. (2015). Mechanical ventilation of acute respiratory distress syndrome. *Journal of Intensive Care*, *3*(1), 1–9. https://doi.org/10.1186/S40560-015-0091-6/FIGURES/2
29. AK, A. K., & Anjum, F. (2022). *Ventilator-Induced Lung Injury (VILI)*. https://www.ncbi.nlm.nih.gov/books/NBK563244/
30. Chen, L., Xia, H. F., Shang, Y., & Yao, S. L. (2018). Molecular Mechanisms of Ventilator-Induced Lung Injury. *Chinese Medical Journal*, *131*(10), 1225. https://doi.org/10.4103/0366-6999.226840
31. Kuhn BT, Nguyen J, Kenyon NJ, Adams JY. Pitfalls in the management of mechanical ventilation: ARDS and hypermetabolic states. Consultant. 2017;57(5):289-292,295.
32. Papazian, L., Klompas, M., & Luyt, C. E. (2020). Ventilator-associated pneumonia in adults: a narrative review. *Intensive Care Medicine*, *46*(5), 888–906. https://doi.org/10.1007/S00134-020-05980-0/TABLES/4
33. Lefebvre, C. W., Babich, J. P., Grendell, J. H., Grendell, J. H., Heffner, J. E., Thibault, R., Pichard, C., Monnet, X., Teboul, J.-L., Sinderby, C. A., Beck, J., Onugha, O. I., Spain, D. A., Bensard, D. D., Partrick, D. A., Asensio, J. A., Verde, J. M., Yeh, D. D., Cohen, M., … Muizelaar, J. P. (2022). Ventilator-associated Pneumonia. *Encyclopedia of Intensive Care Medicine*, 1773–1782. https://doi.org/10.1007/978-3-642-00418-6_91
34. le Pape, M., Besnard, C., Acatrinei, C., Guinard, J., Boutrot, M., Genève, C., Boulain, T., & Barbier, F. (2022). Clinical impact of ventilator-associated pneumonia in patients with

the acute respiratory distress syndrome: a retrospective cohort study. *Annals of Intensive Care*, *12*(1), 1–12. https://doi.org/10.1186/S13613-022-00998-7/FIGURES/3

35. Kalanuria, A. A., Zai, W., & Mirski, M. (2014a). Ventilator-associated pneumonia in the ICU. *Critical Care*, *18*(2), 1–8. https://doi.org/10.1186/CC13775/TABLES/4
36. Alp, E., & Voss, A. (2006). Ventilator associated pneumonia and infection control. *Annals of Clinical Microbiology and Antimicrobials*, *5*, 7. https://doi.org/10.1186/1476-0711-5-7
37. Luyt, C. E., Bouadma, L., Morris, A. C., Dhanani, J. A., Kollef, M., Lipman, J., Martin-Loeches, I., Nseir, S., Ranzani, O. T., Roquilly, A., Schmidt, M., Torres, A., & Timsit, J. F. (2020a). Pulmonary infections complicating ARDS. *Intensive Care Medicine 2020 46:12*, *46*(12), 2168–2183. https://doi.org/10.1007/S00134-020-06292-Z
38. Velásquez-Garcia, L., Mejia-Sanjuanelo, A., Viasus, D., & Carratalà, J. (2022a). Causative Agents of Ventilator-Associated Pneumonia and Resistance to Antibiotics in COVID-19 Patients: A Systematic Review. *Biomedicines 2022, Vol. 10, Page 1226*, *10*(6), 1226. https://doi.org/10.3390/BIOMEDICINES10061226
39. Rodrigues, M. E., Lopes, S. P., Pereira, C. R., Azevedo, N. F., Lourenço, A., Henriques, M., & Pereira, M. O. (2017). Polymicrobial Ventilator-Associated Pneumonia: Fighting In Vitro Candida albicans-Pseudomonas aeruginosa Biofilms with Antifungal-Antibacterial Combination Therapy. *PLoS ONE*, *12*(1). https://doi.org/10.1371/JOURNAL.PONE.0170433
40. Arthur, L. E., Kizor, R. S., Selim, A. G., van Driel, M. L., & Seoane, L. (2016). Antibiotics for ventilator-associated pneumonia. *The Cochrane Database of Systematic Reviews*, *2016*(10). https://doi.org/10.1002/14651858.CD004267.PUB4

41. Wu, D., Wu, C., Zhang, S., & Zhong, Y. (2019). Risk factors of ventilator-associated pneumonia in critically III patients. *Frontiers in Pharmacology*, *10*(MAY), 482. https://doi.org/10.3389/FPHAR.2019.00482/BIBTEX

42. Ventola, C. L. (2015). The Antibiotic Resistance Crisis: Part 1: Causes and Threats. *Pharmacy and Therapeutics*, *40*(4), 277. https://doi.org/Article

43. van Hecke, O., Wang, K., Lee, J. J., Roberts, N. W., & Butler, C. C. (2017). Implications of Antibiotic Resistance for Patients' Recovery From Common Infections in the Community: A Systematic Review and Meta-analysis. *Clinical Infectious Diseases: An Official Publication of the Infectious Diseases Society of America*, *65*(3), 371. https://doi.org/10.1093/CID/CIX233

44. Pang, Z., Raudonis, R., Glick, B. R., Lin, T. J., & Cheng, Z. (2019). Antibiotic resistance in Pseudomonas aeruginosa: mechanisms and alternative therapeutic strategies. *Biotechnology Advances*, *37*(1), 177–192. https://doi.org/10.1016/J.BIOTECHADV.2018.11.013

45. Moretti, M., van Laethem, J., Minini, A., Pierard, D., & Malbrain, M. L. N. G. (2021a). Ventilator-associated bacterial pneumonia in coronavirus 2019 disease, a retrospective monocentric cohort study. *Journal of Infection and Chemotherapy*, *27*(6), 826–833. https://doi.org/10.1016/j.jiac.2021.01.011

46. Mishra B, Singh J. Novel drug delivery systems and significance in respiratory diseases. Targeting Chronic Inflammatory Lung Diseases Using Advanced Drug Delivery Systems. 2020:57–95. doi: 10.1016/B978-0-12-820658-4.00004-2. Epub 2020 Sep 18. PMCID: PMC7499344.

47. He, S., Gui, J., Xiong, K. *et al.* A roadmap to pulmonary delivery strategies for the treatment of infectious lung diseases. *J Nanobiotechnol* 20, 101 (2022). https://doi.org/10.1186/s12951-022-01307-x

48. Prasanna P, Rathee S, Upadhyay A, Sulakshana S. Nanotherapeutics in the treatment of acute respiratory distress syndrome. Life Sci. 2021 Jul 1;276:119428. doi: 10.1016/j.lfs.2021.119428. Epub 2021 Mar 27. PMID: 33785346; PMCID: PMC7999693.

49. Kong, J., Wen, S., Cao, W., Yue, P., Xu, X., Zhang, Y., Luo, L., Chen, T., Li, L., Wang, F., Tao, J., Zhou, G., Luo, S., Liu, A., & Bao, F. (2021). Lung organoids, useful tools for investigating epithelial repair after lung injury. *Stem Cell Research & Therapy 2021 12:1*, *12*(1), 1–13. https://doi.org/10.1186/S13287-021-02172-5

50. Newman, S. P. (2017a). Drug delivery to the lungs: Challenges and opportunities. *Therapeutic Delivery*, *8*(8), 647–661.

51. Foroozandeh, P., & Aziz, A. A. (2018a). Insight into Cellular Uptake and Intracellular Trafficking of Nanoparticles. *Nanoscale Research Letters 2018 13:1*, *13*(1), 1–12. https://doi.org/10.1186/S11671-018-2728-6

52. Löndahl, J., Jakobsson, J. K., Broday, D. M., Aaltonen, H. L., & Wollmer, P. (2017). Do nanoparticles provide a new opportunity for diagnosis of distal airspace disease? *International Journal of Nanomedicine*, *12*, 41. https://doi.org/10.2147/IJN.S121369

53. Boegh, M., & Nielsen, H. M. (2015). Mucus as a Barrier to Drug Delivery – Understanding and Mimicking the Barrier Properties. *Basic & Clinical Pharmacology & Toxicology*, *116*(3), 179–186. https://doi.org/10.1111/BCPT.12342

54. Dong, Y., Zhu, H., Shen, Y., Zhang, W., & Zhang, L. (2019). Antibacterial activity of silver nanoparticles of different particle size against Vibrio Natriegens. *PLoS ONE*, *14*(9). https://doi.org/10.1371/JOURNAL.PONE.0222322

55. Hotze, E. M., Phenrat, T., & Lowry, G. v. (2010). *Nanoparticle Aggregation: Challenges to Understanding Transport and Reactivity in the Environment*. https://doi.org/10.2134/jeq2009.0462

56. He, C., Hu, Y., Yin, L., Tang, C., & Yin, C. (2010). Effects of particle size and surface charge on cellular uptake and biodistribution of polymeric nanoparticles. *Biomaterials*, *31*(13), 3657–3666. https://doi.org/10.1016/J.BIOMATERIALS.2010.01.065

57. Bhattacharjee, S., de Haan, L. H. J., Evers, N. M., Jiang, X., Marcelis, A. T. M., Zuilhof, H., Rietjens, I. M. C. M., & Alink, G. M. (2010). Role of surface charge and oxidative stress in cytotoxicity of organic monolayer-coated silicon nanoparticles towards macrophage NR8383 cells. *Particle and Fibre Toxicology*, *7*(1), 25. https://doi.org/10.1186/1743-8977-7-25/FIGURES/5

58. Hasan, N., Cao, J., Lee, J., Hlaing, S. P., Oshi, M. A., Naeem, M., Ki, M. H., Lee, B. L., Jung, Y., & Yoo, J. W. (2019). Bacteria-Targeted Clindamycin Loaded Polymeric Nanoparticles: Effect of Surface Charge on Nanoparticle Adhesion to MRSA, Antibacterial Activity, and Wound Healing. *Pharmaceutics 2019, Vol. 11, Page 236*, *11*(5), 236. https://doi.org/10.3390/PHARMACEUTICS11050236

59. Link, P. A., Ritchie, A. M., Cotman, G. M., Valentine, M. S., Dereski, B. S., & Heise, R. L. (2018). Electrosprayed extracellular matrix nanoparticles induce a pro-regenerative cell response. *Journal of Tissue Engineering and Regenerative Medicine*, *12*(12), 2331–2336. https://doi.org/10.1002/TERM.2768

60. Kular, J. K., Basu, S., & Sharma, R. I. (2014a). The extracellular matrix: Structure, composition, age-related differences, tools for analysis and applications for tissue engineering. *Journal of Tissue Engineering*, *5*. https://doi.org/10.1177/2041731414557112

61. Kendall, R. T., & Feghali-Bostwick, C. A. (2014a). Fibroblasts in fibrosis: Novel roles and mediators. *Frontiers in Pharmacology*, *5 MAY*, 123. https://doi.org/10.3389/FPHAR.2014.00123/BIBTEX

62. Pompili, S., Latella, G., Gaudio, E., Sferra, R., & Vetuschi, A. (2021a). The Charming World of the Extracellular Matrix: A Dynamic and Protective Network of the Intestinal Wall. *Frontiers in Medicine*, *8*, 477. https://doi.org/10.3389/FMED.2021.610189/BIBTEX

63. Kruegel, J., & Miosge, N. (2010). Basement membrane components are key players in specialized extracellular matrices. *Cellular and Molecular Life Sciences*, *67*(17), 2879. https://doi.org/10.1007/S00018-010-0367-X

64. Frantz, C., Stewart, K. M., & Weaver, V. M. (2010a). The extracellular matrix at a glance. *Journal of Cell Science*, *123*(24), 4195. https://doi.org/10.1242/JCS.023820

65. Ariza de Schellenberger, A., Bergs, J., Sack, I., & Taupitz, M. (2018a). The extracellular matrix as a target for biophysical and molecular magnetic resonance imaging. *Quantification of Biophysical Parameters in Medical Imaging*, 123–150. https://doi.org/10.1007/978-3-319-65924-4_6/FIGURES/5

66. Hackett, T. L., & Osei, E. T. (2021). Modeling Extracellular Matrix-Cell Interactions in Lung Repair and Chronic Disease. *Cells*, *10*(8), 2145. https://doi.org/10.3390/CELLS10082145

67. Karamanos, N. K., Theocharis, A. D., Piperigkou, Z., Manou, D., Passi, A., Skandalis, S. S., Vynios, D. H., Orian-Rousseau, V., Ricard-Blum, S., Schmelzer, C. E. H., Duca, L., Durbeej, M., Afratis, N. A., Troeberg, L., Franchi, M., Masola, V., & Onisto, M. (2021a). A guide to the composition and functions of the extracellular matrix. *The FEBS Journal*, *288*(24), 6850–6912. https://doi.org/10.1111/FEBS.15776

68. Mecham, R. P. (2018). Elastin in Lung Development and Disease Pathogenesis. *Matrix Biology : Journal of the International Society for Matrix Biology*, *73*, 6. https://doi.org/10.1016/J.MATBIO.2018.01.005

69. Ritchie, B. E. (n.d.). *EXTRACELLULAR MATRIX NANOPARTICLES EFFECTS ON THE EXTRACELLULAR MATRIX NANOPARTICLES EFFECTS ON THE LUNG IN VIVO LUNG IN VIVO*. Retrieved January 20, 2023, from https://scholarscompass.vcu.edu/etd

70. Novoseletskaya, E., Grigorieva, O., Nimiritsky, P., Basalova, N., Eremichev, R., Milovskaya, I., Kulebyakin, K., Kulebyakina, M., Rodionov, S., Omelyanenko, N., & Efimenko, A. (2020). Mesenchymal Stromal Cell-Produced Components of Extracellular Matrix Potentiate Multipotent Stem Cell Response to Differentiation Stimuli. *Frontiers in Cell and Developmental Biology*, *8*, 555378. https://doi.org/10.3389/FCELL.2020.555378/FULL

71. Kim, Y. S., Majid, M., Melchiorri, A. J., & Mikos, A. G. (2019). Applications of decellularized extracellular matrix in bone and cartilage tissue engineering. *Bioengineering & Translational Medicine*, *4*(1), 83. https://doi.org/10.1002/BTM2.10110

72. Gilpin, A., & Yang, Y. (2017a). Decellularization Strategies for Regenerative Medicine: From Processing Techniques to Applications. *BioMed Research International*, *2017*. https://doi.org/10.1155/2017/9831534

73. Fernández-Pérez, J., & Ahearne, M. (2019). The impact of decellularization methods on extracellular matrix derived hydrogels. *Scientific Reports 2019 9:1*, *9*(1), 1–12. https://doi.org/10.1038/s41598-019-49575-2

74. Morris, A. H., Stamer, D. K., & Kyriakides, T. R. (2017a). The host response to naturally-derived extracellular matrix biomaterials. *Seminars in Immunology*, *29*, 72–91. https://doi.org/10.1016/J.SMIM.2017.01.002

75. Rabbani, M., Zakian, N., & Alimoradi, N. (2021). Contribution of Physical Methods in Decellularization of Animal Tissues. *Journal of Medical Signals and Sensors*, *11*(1), 1. https://doi.org/10.4103/JMSS.JMSS_2_20

76. Theocharis, A. D., Skandalis, S. S., Gialeli, C., & Karamanos, N. K. (2016). Extracellular matrix structure. *Advanced Drug Delivery Reviews*, *97*, 4–27. https://doi.org/10.1016/J.ADDR.2015.11.001

77. Velez, A. M. A., & Howard, M. S. (2012). Collagen IV in Normal Skin and in Pathological Processes. *North American Journal of Medical Sciences*, *4*(1), 1. https://doi.org/10.4103/1947-2714.92892

78. Wang, K., Meng, X., & Guo, Z. (2021a). Elastin Structure, Synthesis, Regulatory Mechanism and Relationship With Cardiovascular Diseases. *Frontiers in Cell and Developmental Biology*, *9*, 2956. https://doi.org/10.3389/FCELL.2021.596702/BIBTEX

79. Laner-Plamberger, S., Oeller, M., Rohde, E., Schallmoser, K., & Strunk, D. (2021). Heparin and Derivatives for Advanced Cell Therapies. *International Journal of*

Molecular Sciences 2021, Vol. 22, Page 12041, *22*(21), 12041. https://doi.org/10.3390/IJMS222112041

80. Grinnell, F. (1984). Fibronectin and wound healing. *Journal of Cellular Biochemistry*, *26*(2), 107–116. https://doi.org/10.1002/JCB.240260206
81. rownbridge, J. M., & Gallo, R. L. (2002). Dermatan sulfate: New functions from an old glycosaminoglycan. *Glycobiology*, *12*(9). https://doi.org/10.1093/GLYCOB/CWF066
82. Ren, X., Zhao, M., Lash, B., Martino, M. M., & Julier, Z. (2020). Growth Factor Engineering Strategies for Regenerative Medicine Applications. *Frontiers in Bioengineering and Biotechnology*, *7*, 469. https://doi.org/10.3389/FBIOE.2019.00469/BIBTEX
83. Wilgus, T. A. (2012). Growth Factor–Extracellular Matrix Interactions Regulate Wound Repair. *Advances in Wound Care*, *1*(6), 249. https://doi.org/10.1089/WOUND.2011.0344
84. Hynes, R. O. (2009). Extracellular matrix: not just pretty fibrils. *Science (New York, N.Y.)*, *326*(5957), 1216. https://doi.org/10.1126/SCIENCE.1176009
85. Bonnans, C., Chou, J., & Werb, Z. (2014). Remodelling the extracellular matrix in development and disease. *Nature Reviews. Molecular Cell Biology*, *15*(12), 786. https://doi.org/10.1038/NRM3904
86. *Peptides and Skin Health | Linus Pauling Institute | Oregon State University*. (n.d.). Retrieved January 20, 2023, from https://lpi.oregonstate.edu/mic/health-disease/skin-health/peptides
87. de Castro Brás, L. E., & Frangogiannis, N. G. (2020). Extracellular matrix-derived peptides in tissue remodeling and fibrosis. *Matrix Biology*, *91–92*, 176–187. https://doi.org/10.1016/J.MATBIO.2020.04.006

88. Jiménez-Gastélum, G. R., Aguilar-Medina, E. M., Soto-Sainz, E., Ramos-Payán, R., & Silva-Benítez, E. L. (2019). Antimicrobial Properties of Extracellular Matrix Scaffolds for Tissue Engineering. *BioMed Research International*, *2019*.

89. Pittenger, M. F., Discher, D. E., Péault, B. M., Phinney, D. G., Hare, J. M., & Caplan, A. I. (2019). Mesenchymal stem cell perspective: cell biology to clinical progress. *Npj Regenerative Medicine 2019 4:1*, *4*(1), 1–15. https://doi.org/10.1038/s41536-019-0083-6

90. Sadeghian Chaleshtori, S., Mokhber Dezfouli, M. R., & Jabbari Fakhr, M. (2020). Mesenchymal stem/stromal cells: The therapeutic effects in animal models of acute pulmonary diseases. *Respiratory Research*, *21*(1), 1–11. https://doi.org/10.1186/S12931-020-01373-5/TABLES/1

91. Ahangar, P., Mills, S. J., & Cowin, A. J. (2020a). Mesenchymal Stem Cell Secretome as an Emerging Cell-Free Alternative for Improving Wound Repair. *International Journal of Molecular Sciences*, *21*(19), 1–15. https://doi.org/10.3390/IJMS21197038

92. Montero-Vilchez, T., Sierra-Sánchez, Á., Sanchez-Diaz, M., Quiñones-Vico, M. I., Sanabria-de-la-Torre, R., Martinez-Lopez, A., & Arias-Santiago, S. (2021). Mesenchymal Stromal Cell-Conditioned Medium for Skin Diseases: A Systematic Review. *Frontiers in Cell and Developmental Biology*, *9*, 1877. https://doi.org/10.3389/FCELL.2021.654210/BIBTEX

93. Hmadcha, A., Martin-Montalvo, A., Gauthier, B. R., Soria, B., & Capilla-Gonzalez, V. (2020). Therapeutic Potential of Mesenchymal Stem Cells for Cancer Therapy. *Frontiers in Bioengineering and Biotechnology*, *8*, 43. https://doi.org/10.3389/FBIOE.2020.00043/BIBTEX

94. Sandonà, M., di Pietro, L., Esposito, F., Ventura, A., Silini, A. R., Parolini, O., & Saccone, V. (2021). Mesenchymal Stromal Cells and Their Secretome: New Therapeutic Perspectives for Skeletal Muscle Regeneration. *Frontiers in Bioengineering and Biotechnology*, *9*, 319. https://doi.org/10.3389/FBIOE.2021.652970/BIBTEX

95. Marx, C., Gardner, S., Harman, R. M., & van de Walle, G. R. (2020). The mesenchymal stromal cell secretome impairs methicillin-resistant Staphylococcus aureus biofilms via cysteine protease activity in the equine model. *STEM CELLS Translational Medicine*, *9*(7), 746–757. https://doi.org/10.1002/SCTM.19-0333

96. Feng, B., Zhu, J., Xu, Y., Chen, W., Sheng, X., Feng, X., Shi, X., Liu, J., Pan, Q., Yang, J., Yu, J., Li, L., & Cao, H. (2020). Immunosuppressive effects of mesenchymal stem cells on lung B cell gene expression in LPS-induced acute lung injury. *Stem Cell Research and Therapy*, *11*(1), 1–9.

97. Wang, W., Lei, W., Jiang, L., Gao, S., Hu, S., Zhao, Z. G., Niu, C. Y., & Zhao, Z. A. (2021). Therapeutic mechanisms of mesenchymal stem cells in acute respiratory distress syndrome reveal potentials for Covid-19 treatment. *Journal of Translational Medicine 2021 19:1*, *19*(1), 1–13. https://doi.org/10.1186/S12967-021-02862-X

98. Wang F, Li Y, Wang B, Li J, Peng Z. The safety and efficacy of mesenchymal stromal cells in ARDS: a meta-analysis of randomized controlled trials. Crit Care. 2023 Jan 20;27(1):31. doi: 10.1186/s13054-022-04287-4. PMID: 36670442; PMCID: PMC9857915.

99. Mills, C. D. (2012). M1 and M2 Macrophages: Oracles of Health and Disease. *Critical Reviews in Immunology*, *32*(6), 463–488. https://doi.org/10.1615/CRITREVIMMUNOL.V32.I6.10

100. Chen, X., Tang, J., Shuai, W., Meng, J., Feng, J., & Han, Z. (2020). Macrophage polarization and its role in the pathogenesis of acute lung injury/acute respiratory distress syndrome. *Inflammation Research*, *69*(9), 883. https://doi.org/10.1007/S00011-020-01378-2

101. Cao, X., Duan, L., Hou, H., Liu, Y., Chen, S., Zhang, S., Liu, Y., Wang, C., Qi, X., Liu, N., Han, Z., Zhang, D., Han, Z. C., Guo, Z., Zhao, Q., & Li, Z. (2020). IGF-1C hydrogel improves the therapeutic effects of MSCs on colitis in mice through PGE2-mediated M2 macrophage polarization. *Theranostics*, *10*(17), 7697–7709. https://doi.org/10.7150/THNO.45434

102. Lu, D., Xu, Y., Liu, Q., & Zhang, Q. (2021). Mesenchymal Stem Cell-Macrophage Crosstalk and Maintenance of Inflammatory Microenvironment Homeostasis. *Frontiers in Cell and Developmental Biology*, *9*, 1628. https://doi.org/10.3389/FCELL.2021.681171/BIBTEX

103. Papa, S., Vismara, I., Mariani, A., Barilani, M., Rimondo, S., de Paola, M., Panini, N., Erba, E., Mauri, E., Rossi, F., Forloni, G., Lazzari, L., & Veglianese, P. (2018). Mesenchymal stem cells encapsulated into biomimetic hydrogel scaffold gradually release CCL2 chemokine in situ preserving cytoarchitecture and promoting functional recovery in spinal cord injury. *Journal of Controlled Release : Official Journal of the Controlled Release Society*, *278*, 49–56. https://doi.org/10.1016/J.JCONREL.2018.03.034

104. Novoseletskaya, E., Grigorieva, O., Nimiritsky, P., Basalova, N., Eremichev, R., Milovskaya, I., ... & Efimenko, A. (2020). Mesenchymal stromal cell-produced

components of extracellular matrix potentiate multipotent stem cell response to differentiation stimuli. Frontiers in Cell and Developmental Biology, 8, 555378.

105. Chen, X. D., Dusevich, V., Feng, J. Q., Manolagas, S. C., & Jilka, R. L. (2007). Extracellular matrix made by bone marrow cells facilitates expansion of marrow-derived mesenchymal progenitor cells and prevents their differentiation into osteoblasts. *Journal of bone and mineral research*, *22*(12), 1943-1956.

106. White, L. J., Taylor, A. J., Faulk, D. M., Keane, T. J., Saldin, L. T., Reing, J. E., Swinehart, I. T., Turner, N. J., Ratner, B. D., & Badylak, S. F. (2017). The impact of detergents on the tissue decellularization process: A ToF-SIMS study. Acta biomaterialia, 50, 207–219. https://doi.org/10.1016/j.actbio.2016.12.033

107. Gilpin, A., & Yang, Y. (2017a). Decellularization Strategies for Regenerative Medicine: From Processing Techniques to Applications. *BioMed Research International*, *2017*. https://doi.org/10.1155/2017/9831534

108. Songsurang, K., Praphairaksit, N., Siraleartmukul, K., & Muangsin, N. (2011). Electrospray fabrication of doxorubicin-chitosan-tripolyphosphate nanoparticles for delivery of doxorubicin. *Archives of pharmacal research*, *34*, 583-592.

109. Mooney C, Haslam NJ, Pollastri G, Shields DC. Towards the improved discovery and design of functional peptides: common features of diverse classes permit generalized prediction of bioactivity. PLoS One. 2012;7(10):e45012. doi: 10.1371/journal.pone.0045012. Epub 2012 Oct 8. PMID: 23056189; PMCID: PMC3466233.

110. Ge, Q., Chen, L., Jaffar, J. et al. Fibulin1C peptide induces cell attachment and extracellular matrix deposition in lung fibroblasts. Sci Rep 5, 9496 (2015). https://doi.org/10.1038/srep09496

111. Toke, O. (2005). Antimicrobial peptides: new candidates in the fight against bacterial infections. Peptide Science: Original Research on Biomolecules, 80(6), 717-735.

112. Wiesner J, Vilcinskas A. Antimicrobial peptides: the ancient arm of the human immune system. Virulence. 2010 Sep-Oct;1(5):440-64. doi: 10.4161/viru.1.5.12983. PMID: 21178486.

113. Agerberth B, Boman A, Andersson M, Jörnvall H, Mutt V, Boman HG. Isolation of three antibacterial peptides from pig intestine: gastric inhibitory polypeptide (7-42), diazepam-binding inhibitor (32-86) and a novel factor, peptide 3910. Eur J Biochem. 1993 Sep 1;216(2):623-9. doi: 10.1111/j.1432-1033.1993.tb18182.x. PMID: 8375398.

114. Halper, J., & Kjaer, M. (2014). Basic components of connective tissues and extracellular matrix: elastin, fibrillin, fibulins, fibrinogen, fibronectin, laminin, tenascins, and thrombospondins. *Progress in heritable soft connective tissue diseases*, 31-47.

115. Wu, Y. L., Lin, C. W., Cheng, N. C., Yang, K. C., & Yu, J. (2017). Modulation of keratin in adhesion, proliferation, adipogenic, and osteogenic differentiation of porcine adipose-derived stem cells. *Journal of Biomedical Materials Research Part B: Applied Biomaterials*, *105*(1), 180-192.

116. Zhang, K., Li, M., Yin, L., Fu, G., & Liu, Z. (2020). Role of thrombospondin-1 and thrombospondin-2 in cardiovascular diseases. *International journal of molecular medicine*, *45*(5), 1275-1293.

117. Argraves WS, Greene LM, Cooley MA, Gallagher WM. Fibulins: physiological and disease perspectives. EMBO Rep. 2003 Dec;4(12):1127-31. doi: 10.1038/sj.embor.7400033. PMID: 14647206; PMCID: PMC1326425.

118. Al-Talib, H., Abdulwahab, M. H., Murad, K., Amiruddin, N. D., & Mohamed, N. N. (2023). Antimicrobial Effects of Tetraspanin CD9 Peptide against Microbiota Causing Armpit Malodour. *Antibiotics*, *12*(2), 271.

119. Karam, J., Méresse, S., Kremer, L., & Daher, W. (2020). The roles of tetraspanins in bacterial infections. *Cellular Microbiology*, *22*(12), e13260.

120. Rodziewicz-Motowidło, S., Mickiewicz, B., Greber, K., Sikorska, E., Szultka, Ł., Kamysz, E., & Kamysz, W. (2010). Antimicrobial and conformational studies of the active and inactive analogues of the protegrin-1 peptide. *The FEBS journal*, *277*(4), 1010-1022.

121. Gabay, J. E., & Almeida, R. P. (1993). Antibiotic peptides and serine protease homologs in human polymorphonuclear leukocytes: defensins and azurocidin. *Current opinion in immunology*, *5*(1), 97-102.

122. Craven, T. H., Avlonitis, N., McDonald, N., Walton, T., Scholefield, E., Akram, A. R., ... & Dhaliwal, K. (2018). Super-silent FRET sensor enables live cell imaging and flow cytometric stratification of intracellular serine protease activity in neutrophils. *Scientific reports*, *8*(1), 13490.

123. AGERBERTH, B., BOMAN, A., ANDERSSON, M., JÖRNVALL, H., MUTT, V., & BOMAN, H. G. (1993). Isolation of three antibacterial peptides from pig intestine: gastric inhibitory polypeptide (7–42), diazepam-binding inhibitor (32–86) and a novel factor, peptide 3910. *European journal of biochemistry*, *216*(2), 623-629.

124. Sveiven, S. N., & Nordgren, T. M. (2020). Lung-resident mesenchymal stromal cells are tissue-specific regulators of lung homeostasis. *American Journal of Physiology-Lung Cellular and Molecular Physiology*, *319*(2), L197-L210.

125. Addis R, Cruciani S, Santaniello S, Bellu E, Sarais G, Ventura C, Maioli M, Pintore G. Fibroblast Proliferation and Migration in Wound Healing by Phytochemicals: Evidence for a Novel Synergic Outcome. Int J Med Sci. 2020 Apr 7;17(8):1030-1042. doi: 10.7150/ijms.43986. PMID: 32410832; PMCID: PMC7211158.

126. Rasband, W.S., ImageJ, U. S. National Institutes of Health, Bethesda, Maryland, USA, https://imagej.nih.gov/ij/, 1997-2018.

127. AGERBERTH, B., BOMAN, A., ANDERSSON, M., JÖRNVALL, H., MUTT, V., & BOMAN, H. G. (1993). Isolation of three antibacterial peptides from pig intestine: gastric inhibitory polypeptide (7–42), diazepam-binding inhibitor (32–86) and a novel factor, peptide 3910. *European journal of biochemistry*, *216*(2), 623-629.

128. Novoseletskaya, E., Grigorieva, O., Nimiritsky, P., Basalova, N., Eremichev, R., Milovskaya, I., ... & Efimenko, A. (2020). Mesenchymal stromal cell-produced components of extracellular matrix potentiate multipotent stem cell response to differentiation stimuli. *Frontiers in Cell and Developmental Biology*, *8*, 555378.

129. Kendall, R. T., & Feghali-Bostwick, C. A. (2014). Fibroblasts in fibrosis: novel roles and mediators. *Frontiers in pharmacology*, *5*, 123.

130. Ito Y, Correll K, Schiel JA, Finigan JH, Prekeris R, Mason RJ. Lung fibroblasts accelerate wound closure in human alveolar epithelial cells through hepatocyte growth factor/c-Met signaling. Am J Physiol Lung Cell Mol Physiol. 2014 Jul 1;307(1):L94-105.

doi: 10.1152/ajplung.00233.2013. Epub 2014 Apr 18. PMID: 24748602; PMCID: PMC4080284.

131. Schmidt NW, Wong GC. Antimicrobial peptides and induced membrane curvature: geometry, coordination chemistry, and molecular engineering. Curr Opin Solid State Mater Sci. 2013 Aug;17(4):151-163. doi: 10.1016/j.cossms.2013.09.004. PMID: 24778573; PMCID: PMC4000235.

132. Epand, R. M., Walker, C., Epand, R. F., & Magarvey, N. A. (2016). Molecular mechanisms of membrane targeting antibiotics. *Biochimica et Biophysica Acta (BBA)-Biomembranes*, *1858*(5), 980-987.

133. Epand, R. M., & Epand, R. F. (2011). Bacterial membrane lipids in the action of antimicrobial agents. *Journal of Peptide Science*, *17*(5), 298-305.

Vita

Emily N. Wandling

10451 Atlee Station Road, Apt 404, Mechanicsville, VA 23116
(804) 572-8774
wandlingen@vcu.edu
LinkedIn: linkedin.com/in/emily-wandling/

Biomedical Engineering Graduate Student at VCU researching nanoparticles, extracellular matrix, biomaterials, and lung disease in preparation for a career in the Biomaterials Industry

EDUCATION

Bachelor of Science, Biochemistry and Molecular Biology **May 2020**
Sweet Briar College, Sweet Briar, VA

- Graduated summa cum laude with departmental honors
- 3.99/4.00 cumulative GPA

Master of Science, Biomedical Engineering **Spring 2023**
Virginia Commonwealth University, Richmond, VA

- Member of the Heise Pulmonary Mechanobiology Lab
- Master's Thesis: *The Wound Healing and Antibacterial effects of Mesenchymal Stromal Cell Extracellular Matrix Nanoparticles*
- 4.0/4.0 cumulative GPA

RESEARCH

2021-2023 Fabricated a nanoparticle made of extracellular matrix (ECM) proteins from mesenchymal stromal cells. Adapted a decellularization protocol to obtain ECM from mouse mesenchymal stromal cells (MMSC). Optimized electrospray deposition protocol to make the MMSC ECM nanoparticles. Analyzed the size, zeta potential, and proteins found in the nanoparticles using the zetasizer and mass spectroscopy. The biocompatibility of the nanoparticles was evaluated using the MTT assay with MLE-12 cells and MMSCs. The wound healing abilities of the nanoparticles were evaluated using the scratch assay with human lung fibroblasts. Antibacterial effects of the nanoparticles were evaluated against *Escherichia coli, Staphylococcus aureus*, and *Pseudomonas aeruginosa*. Conducted research for Master's Thesis under the guidance of Rebecca L. Heise and Dennis E. Ohman.

Fall 2019-2020 Completed acetylation of betulin to yield diacetylated betulin, Created purification procedure for diacetylated betulin using recrystallization

techniques, analyzed diacetylated betulin derivative using NMR spectroscopy, IR spectroscopy, Thin Layer Chromatography, and Elemental Analysis, Tested the thermal stability of diacetylated betulin, Conducted research as Senior Honors Thesis under the guidance of Dr. Abraham Yousef and Dr. Michael R. Davis Jr., Successfully Defended Honors Thesis against Faculty Committee and Awarded Highest Honors

Summer 2019 Optimized the purification protocol of betulin, Attempted benzylation of betulin, Conducted dehydration of betulin to yield dehydrated allobetulin, Analyzed the dehydrated allobetulin derivative using NMR spectroscopy, IR spectroscopy, and Thin Layer and Column Chromatography, Conducted research as Sweet Briar College Summer Honors Fellow under the guidance of Dr. Abraham Yousef and Dr. Michael R. Davis Jr.

Fall 2019 Attempted esterification of betulin to yield a betulin ester (28-*O*-(*p*-chlorobenzyl)betulin), Analyzed derivative with NMR Spectroscopy, IR Spectroscopy, and Thin Layer Chromatography, Tested antimicrobial properties of betulin against *Pseudomonas aeruginosa* with 96-well assay, Conducted research as Sweet Briar Chemistry Intern under the guidance of Dr. Abraham Yousef, Dr. Michael R. Davis Jr., and Dr. Rob Granger II

Summer 2018 Optimized the Soxhlet extraction protocol of betulin from paper birch bark, Attempted oxidation of betulin to yield betulinic acid and betulonic acid, Used Thin Layer Chromatography, NMR Spectroscopy, and IR Spectroscopy to analyze betulin and betulin derivatives, Tested antimicrobial properties of betulin against *P. aeruginosa* with Kirby-Bauer Assay, Conducted research as Sweet Briar College Summer Honors Fellow under the guidance of Dr. Abraham Yousef and Dr. Michael R. Davis Jr.

PAPERS/PRESENTATIONS

2023 **Wandling, E.N.,** Rhoads, K., Moore, K. Ohman, D.E., & Heise, R.L. (2023). The Wound Healing and Antibacterial Effects of Mesenchymal Stromal Cell Extracellular Matrix Nanoparticles. (2023) Virginia Commonwealth University Master's Thesis.

2023 **Wandling, E.N.,** Rhoads, K., Moore, K. Ohman, D.E., & Heise, R.L. (2023). Electrosprayed Mesenchymal Stromal Cell Extracellular Matrix Nanoparticles Possess Wound Healing and Antimicrobial Effects. *Pharmaceutics.* Publication Accepted and Pending.

2023	**Wandling, E.N.,** Rhoads, K., Moore, K. Ohman, D.E., & Heise, R.L. (2023). "The Wound Healing and Antibacterial Effects of Mesenychmal Stromal Cell Extracelluar Matrix Nanoparticles" at Society of Biomaterials 2023 Meeting in San Diego, California
2022	Kamga Gninzeko, F. J., Tho, C. K., Valentine, M. S., **Wandling, E. N.,** & Heise, R. L. (2022). Mechanical Ventilation induced DNA Damage and P21 in an Acute Aging Model of Lung Injury. *bioRxiv*, 2022-03.
2020	**Wandling, E.N.,** Yousef, A. L., & Davis, M. R. Jr. (2020). Synthesis of Betulin Analogue; Sweet Briar College Departmental Honors Thesis
2019	**Wandling, E. N.,** Yousef, A. L., & Davis, M. R. Jr. Presented "Synthesis of Betulin Derivative" at Mid-Atlantic Regional Conference of Undergraduate Scholarship at Randolph College
2019	**Wandling, E. N.,** Yousef, A. L., & Davis, M. R. Jr. (2019). Extraction of Betulin and Synthesis of Betulin Analogue; Sweet Briar College Summer Honors Research Program
2019	**Wandling, E. N.,** Atkins, C. L., Yousef, A. L., & Davis, M. R. Jr. Presented "Extraction of Betulin and Synthesis of a Betulin Analogue" at National American Chemical Society Conference in Orlando, Florida
2018	**Wandling, E. N.,** Yousef, A. L., & Davis, M. R. Jr. Presented "Extraction and Oxidation of Betulin" at Mid-Atlantic Regional Conference of Undergraduate Scholarship at Sweet Briar College
2018	**Wandling, E. N.,** Yousef, A. L., & Davis, M. R. Jr. (2018). Extraction and Oxidation of Betulin; Sweet Briar College Summer Honors Research Program

TEACHING EXPERIENCE

Virginia Commonwealth University (Richmond, VA)

2021-2022	Taught High School Student Volunteer cell culture and electrospray laboratory techniques.

Sweet Briar College (Sweet Briar, VA)

Fall 2019	Chemistry Teaching Assistant- Organic Chemistry II Lab
Fall 2018	Chemistry Teaching Assistant- General Chemistry Lab
Fall 2017	Chemistry Teaching Assistant-General Chemistry Lab
2018-2020	Chemistry, Biology and Mathematics Departmental Tutor

HONORS AND AWARDS

2021	Virginia Commonwealth University Graduate Master's Scholarship
2021	NSF Graduate Research Fellowship Program Honorable Mention Award
2020	James Lewis Howe Senior Excellence Award in Chemistry
2020	Centra Health Award for Scientific Research and Collaborative Innovation
2020	Judith Molinar Elkins Award: Achievement in Sciences and Student Life
2020	ODAC/Virginia Farm Bureau Insurance Scholar-Athlete of the Year
2020	Sweet Briar Chrysler Award for Leadership and Involvement in Athletics
2019-2020	VaSID Academic All-State Team
2019-2020	Google Cloud Academic All-District Team
2019	Nancy Godwin Baldwin '57 Scholar
2019	Sweet Briar College Whiteman-Scholar Athlete of the Year
2019	2nd-Tennis Team All-ODAC
2018	Sweet Briar College Manson Memorial Scholarship
2018	Sweet Briar College Class of 1977 Sportsmanship Award
2017	Susan Piepho 1st-Year Excellence Award in Chemistry
2017-2020	ITA Scholar-Athlete
2017-2020	ODAC All-Academic Tennis Team
2016	Sweet Briar College Presidential Scholarship
2016	Sweet Briar College Prothro Scholarship
2016-2020	Dean's List

PROFESSIONAL EXPERIENCE

June 2022-present — Product Development Intern, Tympanogen Inc, Richmond, VA

- Developed design verification testing for novel product
- Performed laboratory testing for characterization of gel product
- Supervised performance of FDA Biocompatibility testing for product

July 2020-June 2022 — Medical Technologist, Genetworx, Richmond, VA

- Performed /PCR testing for SARS-CoV-2 and variants

PROFESSIONAL MEMBERSHIPS

2022	Society of Biomaterials Student Member
2020	Chi Alpha Sigma Student-Athlete Honors Society
2019	Omicron Delta Kappa Leadership Honors Society
2019	Iota Sigma Pi Chemistry Honors Society
2019	Eta Sigma Pi Latin Honors Society

2017 Alpha Lambda Delta Honors Society
2017 American Chemical Society

EXTRACURRICULAR AND VOLUNTEER EXPERIENCES

2021-2023 Engineering Graduate Student Association, *VCU*
- Treasurer, *2022-2023*
- Organized professional and social events for the graduate student community at Virginia Commonwealth University

2021-2023 Student Volunteer for VCU Engineering Outreach
- Volunteered at elementary school events to introduce students to biomedical engineering.
- Taught High School Students Cell Culture and Media Change Techniques.

2019-2020 Rehab Associates of Central Virginia, *Amherst, VA*
- Physical Therapy Volunteer
- Observed patient evaluations and routines
- Helped patients with exercises under the supervision of a licensed physical therapist
- Cleaned gym equipment and completed clinic laundry and maintenance

2017-2020 Service Learning Program, *Sweet Briar College*
- Organized and planned Brownie Science Day, an event to introduce elementary-aged girl scouts to science and STEM fields

2017-2020 Tau Phi Academic Honor Club, *Sweet Briar College*
- President, *2019-2020,* Treasurer, *2018-2019*
- Planned study halls to encourage academic success on campus

2017-2020 BAM Community Service Club, *Sweet Briar College*

2017-2020 Falls on Nose School Spirit and Community Service Club
- Treasurer, *2017-2019, Sweet Briar College*

2016-2020 Student-Athlete Advisory Committee, *Sweet Briar College*
- Vice President, *2018-2020*
- Planned events to increase awareness of athletics on campus and of women in sports
- Organized “Pie a Professor Event” to raise money for the organization Walk for Water
- Hosted annual Angel tree drive to donate essential items to Lynchburg’s Women’s shelter

2016-2020 Student Affiliate of the American Chemical Society, *Sweet Briar College*
- President, *2018-2020,* Vice President, *2017-2018,* Treasurer, *2016-2017*
- Created events to raise awareness towards scientific research

SKILLS

Spectral Analysis	NMR analysis (including ^{1}H and ^{13}C NMR, COSY, HETCOR, DEPT), IR Spectroscopy, GC-MS, UV-Vis, HPLC, Fluorometric analysis, Mass Spectroscopy
Cell Culture	Mammalian Cell Culture, Bacterial Cell Culture, Bacterial Plate Spreading
Biological Assays	Kirby-Bauer Assay, ELISA, Sircol Collagen Assay, Blyscan Glycosaminoglycan Assay, Picogreen Assay, MTT Assay, Scratch Assay
Computer	MATLAB, Python, R, Pymol, JASP, Microsoft Office
Molecular Lab	Experience using Eppendorf, ARIES, Bio-Rad, KingFisher Flex, Oktopure, and IntelliQube instruments to extract genetic material and conduct PCR testing for SARS-CoV-2
Gel Electrophoresis	Agarose gel, SDS-PAGE
Chromatography	Thin-Layer Chromatography, Column Chromatography
Staining Techniques	Gram, Endospore, Acid-fast, Capsule
Differential and Selective Media	Mannitol Salt Agar, MacConkey's Agar, Hektoen Enteric Agar, Triple Sugar Iron, Starch Agar, Simmons Citrate Slants, Phenol Red, SIM, LIA
Languages	Latin, Italian (elementary)